

This item is the archived peer-reviewed author-version of:

CO_2 conversion by plasma technology : insights from modeling the plasma chemistry and plasma reactor design

Reference:

Bogaerts Annemie, Berthelot Antonin, Heijkers Stijn, Kolev Stanimir, Snoeckx Ramses, Sun Surong, Trenchev Georgi, Van Laer Koen, Wang Weizong.- CO_2 conversion by plasma technology : insights from modeling the plasma chemistry and plasma reactor design
Plasma sources science and technology / Institute of Physics [Londen] - ISSN 0963-0252 - Bristol, IOP Publishing Ltd, 26:6(2017), 063001
Full text (Publisher's DOI): <https://doi.org/10.1088/1361-6595/AA6ADA>
To cite this reference: <http://hdl.handle.net/10067/1444290151162165141>

CO₂ conversion by plasma technology: Insights from modeling the plasma chemistry and plasma reactor design

A. Bogaerts¹, A. Berthelot¹, S. Heijkers¹, St. Kolev², R. Snoeckx¹, S. Sun¹, G. Trenchev¹, K. Van Laer¹ and W. Wang¹

¹Research group PLASMANT, Department of Chemistry, University of Antwerp, Universiteitsplein 1, B-2610 Wilrijk-Antwerp, Belgium

²Faculty of Physics, Sofia University, 5 James Bourchier Boulevard, 1164 Sofia, Bulgaria

E-mail: annemie.bogaerts@uantwerpen.be

Abstract

In recent years there is growing interest in the use of plasma technology for CO₂ conversion. To improve this application, a good insight in the underlying mechanisms is of great importance. This can be obtained from modeling of the detailed plasma chemistry, to understand the chemical reaction pathways leading to CO₂ conversion (either in pure form or mixed with another gas). Moreover, in practice several plasma reactor types are being investigated for CO₂ conversion, so in addition it is essential to model these reactor geometries, in order to be able to improve their design, and to achieve the most energy efficient CO₂ conversion. Modeling the detailed plasma chemistry of CO₂ conversion in complex reactors is, however, very time-consuming. This problem can be overcome by using a combination of two different types of models. 0D chemical reaction kinetics models are very suitable for describing the detailed plasma chemistry, while the characteristic features of different reactor geometries can be studied by 2D or 3D fluid models. The latter can in first instance be developed in argon or helium, with a simple chemistry, to limit the calculation time, but the ultimate aim is to implement the more complex CO₂ chemistry in these models. In the present paper, examples will be given of both 0D plasma chemistry models and 2D and 3D fluid models for the most common plasma reactors used for CO₂ conversion, to emphasize the complementarity of both approaches. Furthermore, based on the modeling insights, the paper discusses the possibilities and limitations of plasma-based CO₂ conversion in the different types of plasma reactors, and what would be needed to make further progress in this field.

1. Introduction

Global warming is one of the major problems of the 21st century. To solve this problem, the atmospheric CO₂ concentration needs to be drastically reduced. Several initiatives are being taken, such as reducing the CO₂ emissions, among others by increasing the overall energy efficiency of various processes, using more sustainable energy sources instead of burning fossil fuels, but also carbon capture and storage (CCS) or utilization (CCU). The latter is particularly interesting, because the CO₂ can be converted into value-added chemicals, which can be used as feedstock for the chemical industry or as renewable fuels. This conversion might thus simultaneously solve two important problems, i.e., global warming, but also our dependence on fossil feedstocks for transport, energy and as building blocks in the chemical industry. Furthermore, turning a waste product like CO₂ into new feedstock fits in the framework of green chemistry and also complies with the revolutionary “cradle-to-cradle” principle [1].

A lot of research is performed towards energy efficient conversion technologies, such as thermal catalysis, electrocatalysis, photocatalysis, bioelectrocatalysis, etc (e.g., [2-4]). In recent years, there is also growing interest for plasma and plasma catalysis as a possible energy-efficient alternative, because the conversion can proceed at mild reaction conditions. Indeed, the gas does not have to be heated as a whole, because the electrons can activate the gas by electron impact excitation, dissociation and ionization. Moreover, as plasma can easily be switched on/off, it also has great potential for the temporary storage of excess renewable energy during peak production. Thus, plasma technology can contribute to the solution for a third major problem of the 21st century, i.e., the integration of intermittent renewable energy into the existing electricity grid, and thus to provide a solution for the current imbalance between the supply and demand of energy, by using the excess renewable energy for the conversion of CO₂ into new fuels.

However, more basic research is still essential before plasma technology can be successfully applied for this application. This is possible through experiments, but also by modeling the plasma chemistry for CO₂ conversion and by modeling the plasma reactors typically used for this purpose.

The most commonly used plasma reactor types for CO₂ conversion are (packed bed) dielectric barrier discharges (DBDs) [5-18], microwave (MW) plasmas [19-24] and low-current non-thermal gliding arc (GA) discharges [25-33], although ns-pulsed [34] and spark discharges [35-37] have also been employed. There is a clear need for more detailed modeling of these plasma reactor types, to reveal their characteristic features, and to better understand how these features affect their energy efficiency. Indeed, the energy efficiency of CO₂ conversion is one of the major criteria in the search for optimal plasma reactor design. The highest energy efficiency up to now was reported for a MW plasma, i.e., up to 90% [19], but it is important to realise that this was obtained under very specific conditions, *viz.* supersonic gas flow and reduced pressure (~100-200 Torr), and increasing the pressure to 1 atm, which is desirable for industrial applications, causes a significantly lower energy efficiency, e.g., around 40% at normal flow conditions and atmospheric pressure [37]. Moreover, such high values have not yet been reproduced since then. The highest energy efficiency reported more recently for a MW plasma was 55% [22], but this was again at reduced pressure and supersonic flow. Furthermore, an energy efficiency of 50% was recently obtained for a MW plasma at atmospheric pressure, by applying a reverse vortex flow [23]. A GA plasma also exhibits a rather high energy efficiency, even at atmospheric pressure, i.e., around 30-35 % for a conversion of about 10 % in the case of CO₂ splitting, as obtained in a reverse vortex flow (RVF) GA [27,33], and even around 60% for a conversion of 8-16%, for dry reforming of methane (DRM) [29]. Moreover, the combination of a GA plasma with catalysts in a heat-insulated reactor has shown to yield a dramatic rise in energy efficiency (up to 86%) with a CH₄ conversion of 92 % and a CO₂ conversion of 23% [32]. The energy efficiency of a DBD is more limited, i.e., up to 10% for a CO₂ conversion of 30% (e.g., [16]), but this value can be improved by inserting a (dielectric) packing into the reactor, yielding a so-called packed bed DBD reactor (e.g., [14,18]). Moreover, when the packing is catalytically active, it enables the selective production of targeted compounds, in so-called plasma catalysis (e.g., [7-9,12,13]). Furthermore, a DBD reactor typically operates at atmospheric pressure and has a very simple design, making it suitable for upscaling. Therefore, it also has potential for industrial applications.

To investigate which reactor designs can lead to improved CO₂ conversion, 2D or even 3D fluid models are probably the most suitable approaches, in terms of a compromise between level of detail and calculation time. However, such fluid models still require a long calculation time, certainly in case of complex geometries or gas flow patterns (e.g., supersonic flow or reverse vortex flow), which are of interest for improved CO₂ conversion, as mentioned above. Therefore, to our knowledge, there exist no 2D or 3D models yet for describing CO₂ conversion. The fluid models that have been developed up to now in literature for the above types of plasma reactors are typically developed for argon or helium, or sometimes for air, with limited chemistry.

For packed bed DBD reactors, different types of modeling approaches can be found in literature. Chang [38] applied a 0D plasma chemistry model, simply predicting the enhancement factor of the electric field in the voids between the ferroelectric pellets from the ratio of the dielectric constant of the pellets and the gas phase, while Takaki et al. [39] developed a simplified time-averaged 1D model for N_2 , based on solving the transport equations and Poisson's equation. Ya et al. [40] developed a 2D particle-in-cell / Monte Carlo collision (PIC/MCC) model to describe the filamentary discharge behavior in a parallel-plate packed bed DBD reactor in air. Furthermore, some 2D fluid modelling efforts have also been reported. Kang et al. [41] developed a 2D model of a DBD reactor with two stacked ferroelectric beads inside, studying the propagation of the microdischarges during the first 20 ns, and describing the behavior of electrons and ions by a set of fluid equations, but no plasma chemical species were taken into account. Russ et al. [42] applied a 2D fluid model to simulate transient microdischarges in a packed bed DBD reactor filled with dry exhaust gas, but only focusing on a short discharge (few tens of nanoseconds). Kushner and coworkers [43] recently presented 2D fluid model simulations for a packed bed reactor constructed out of dielectric rods, in humid air, studying in detail the mechanism of discharge propagation, while Van Laer et al. [44,45] developed two complementary 2D fluid models to describe a packed bed DBD reactor in helium.

For MW plasmas, there exist a large number of modeling approaches in literature, in various levels of detail, and a recent overview was presented in [46]. Self-consistent 2D fluid models, solving the Maxwell equations for the electromagnetic field and a set of plasma fluid equations, assuming ambipolar diffusion, have been developed by van Dijk, van der Mullen and coworkers [47-49] and by Graves, Moisan and coworkers [50]. Some of these models were applied to atmospheric pressure cylindrical (surfaguide or surfatron) MW plasmas [48,50], while others were applied to intermediate pressure coaxial microwave discharges [49]. These models are very valuable, but they were not applied in the context of CO_2 conversion. Recently, a comparison between two fluid models, based on the coupled solution of the species conservation equations and Poisson's equation (i.e., so-called non-quasi-neutral approach) on the one hand, and on a quasi-neutral approach on the other hand, was presented at intermediate pressure, again for argon, but with the intention to extend it to CO_2 [46]. Finally, Chen et al. showed calculated 2D electron density and electron temperature profiles, again in an argon MW plasma obtained by a quasi-neutral fluid approach, but in the context of catalyst activation for CO_2 decomposition [51].

For low-current non-thermal GA discharges (typically near 1 A or below), some simple 1D analytical or semi-analytical models have been developed [52-57], such as the so-called plasma string model [52] and the Elenbaas-Heller model, assuming an equilibrium plasma and the radius of the plasma channel to be constant [53-55] or with a correction based on an analytical relation between the electric field and the electron and gas temperatures for a non-equilibrium plasma [56]. Some studies also focused on the calculation of the discharge electrical parameters [57]. However, these simple models do not include a detailed chemistry, and they cannot describe the complex behavior of the GA, including unsteady behavior in time and space, arc restrike, non-equilibrium effects, effects of flow patterns, etc., so they inevitably cause a large deviation from the actual situation. Recently, Gutsol and Gangoli presented a simple 2D model of a GA, in the plane parallel to the gas flow and perpendicular to the discharge current, providing very useful information about the gas-discharge interaction [58]. Within our group, we also developed a 2D non-quasi-neutral fluid model to study the arc gliding process in an argon GA [59], and we compared the glow and arc mode in this setup [60]. Moreover, we also presented a 2D quasi-neutral model [61], and this approach was also applied in 3D modelling for a classical (diverging electrode) GA [62] and a RVF GA (also called GA plasmatron; GAP) [63]. These models were all developed for argon, but recently, we also presented a 0D model [64] and a 1D model [65] for a GA in CO_2 , considering the detailed plasma chemistry of CO_2 conversion. Furthermore, Indarto et al. have also presented a 0D model for a GA, describing the chemistry of CH_4 conversion [66,67].

Describing a detailed plasma chemistry in 2D or 3D models, with 100s of species and chemical reactions, is currently not yet feasible, as it would yield excessively long calculation times. For this purpose, 0D plasma chemistry modeling is much more suitable, to elucidate the underlying chemical reaction pathways. Already in the 80s and 90s of previous century, some papers were published on CO₂ plasma chemistry modeling, albeit for applications to CO₂ lasers [68-70]. Furthermore, some papers studied the vibrational kinetics of CO₂ for gas flow applications, although not with focus on the plasma chemistry [71,72]. Rusanov, Fridman and Sholin were the first to develop a model for CO₂ conversion in a MW plasma, based on particle and energy conservation equations for the neutral species, as well as an analytical description of the vibrational distribution function [73]. This model was able to predict a CO₂ conversion and energy efficiency in good agreement with experimental data, but it did not yet include the full plasma chemistry with charged species and a self-consistent calculation of the electron density.

In the last two decades, quite some plasma chemistry models have been developed in literature, for pure CO₂ splitting [16,64,65,74-89], but also in CH₄ (which is of interest for hydrocarbon reforming) [66,67,90,91], as well as in various mixtures, such as CO₂/CH₄ [92-104], CH₄/O₂ [104-110], CO₂/H₂O [111] and CO₂/H₂ [7,112]. Indeed, mixtures of CO₂ with a H-source gas, such as CH₄, H₂O or H₂, are being investigated in order to produce a variety of value-added chemicals, such as syngas (CO/H₂ mixture), which can be used in Fischer-Tropsch synthesis for the production of liquid hydrocarbons. Moreover, the direct formation of oxygenates and higher hydrocarbons by plasma technology is being investigated as well. Furthermore, some papers have focused on modeling the plasma chemistry in CO₂/N₂ [113,114] or CH₄/N₂ [115-120] mixtures. These mixtures are indeed of great interest, because N₂ is a major component in effluent gases, and investigating these mixtures can reveal whether toxic (NO_x) compounds would be formed in the presence of N₂, or vice versa, whether this provides potential for N-fixation if sufficiently high concentrations of these compounds could be formed. It should be noted that most of the above studies are based on 0D chemical kinetics models, although some are based on 1D fluid modeling.

In the following, a brief description of both 0D chemical kinetics modeling, applied to CO₂ or CH₄ conversion and the above-mentioned mixtures, as well as 2D or 3D fluid modeling approaches for the various plasma reactors of interest for CO₂ conversion, will be presented. Subsequently, some typical modeling results will be illustrated, mainly from our own work, but complemented with some data from literature. We will show that these modeling results can give more insights in the underlying mechanisms, and can reveal the possibilities and limitations for CO₂ conversion (and its mixtures) in various types of plasmas. Finally, in the conclusion, we will give an outlook for future modeling needs, to make further progress in this field, and we will also make an assessment of the most suitable reactor and reaction conditions for CO₂ conversion, based on the modeling insights presented in this paper. Finally, based on these results, we will indicate whether plasma technology can be competitive with other emerging CO₂ conversion technologies.

2. Model description

2.1. 0D chemical kinetics modeling

As mentioned above, studying a detailed plasma chemistry is most convenient by means of 0D plasma chemistry models, as they allow to describe a large number of species, and incorporate a large number of chemical reactions, with limited computational effort. A 0D chemical kinetics model is based on solving balance equations for all the species densities, based on production and loss rates, as defined by the chemical reactions:

$$\frac{dn_i}{dt} = \sum_j \left\{ (a_{ij}^{(2)} - a_{ij}^{(1)}) k_j \prod_l n_l^{a_{lj}^{(1)}} \right\}$$

where $a_{ij}^{(1)}$ and $a_{ij}^{(2)}$ are the stoichiometric coefficients of species i , at the left and right hand side of a reaction j , respectively, n_l is the species density at the left-hand side of the reaction, and k_j is the rate coefficient of reaction j (see below).

Table 1 illustrates the species typically included in such models, for either pure CO_2 , pure CH_4 , as well as the extra species included in CO_2/CH_4 , $\text{CO}_2/\text{H}_2\text{O}$, CO_2/H_2 or CH_4/O_2 gas mixtures, and in CO_2/N_2 and CH_4/N_2 mixtures. Note that the same species can be included in the CO_2/CH_4 , $\text{CO}_2/\text{H}_2\text{O}$, CO_2/H_2 and CH_4/O_2 models, because these combinations indeed yield the production of similar molecules. For the CO_2/N_2 and CH_4/N_2 mixtures, again mostly the same species can be included in the model, but with some exceptions. Details of these chemistries for the specific gas mixtures can be found e.g. in [16,74-76,100-102,104,111-114,120].

As the vibrational levels of CO_2 can play an important role in energy-efficient CO_2 conversion, at least in MW and GA plasmas [121], a lot of attention should be paid to a detailed description of the vibrational kinetics of CO_2 , especially when modelling MW or GA conditions. This is especially true for the asymmetric stretch mode of CO_2 , because the latter is considered as the most important channel for dissociation [121]. Additionally, when modelling a CO_2/N_2 mixture in a MW or GA plasma, it is also important to incorporate the N_2 vibrational levels, which turn out to be important for populating the CO_2 vibrational levels in a MW plasma [113]. Furthermore, also the CO vibrational levels are typically taken into account, up to level 10 (see Table 1). They are, however, not so important at the conditions under study, although the first levels of CO can have a minor influence on the CO_2 conversion. Besides, 4 CO electronically excited states are included in Table 1, but they don't have much effect. Indeed, in the reduced chemistry model that we developed for the MW plasma [85], we could remove both the vibrationally and electronically excited states of CO without affecting the results. On the other hand, the vibrational levels of O_2 are more important for studying the CO_2 conversion, since the dissociation of O_2 creates an O atom, which can react with another CO_2 molecule, and thus enhance the overall conversion. Therefore, some of the lowest O_2 vibrational levels with the highest population should also be included in models for CO_2 conversion, at least for a MW and GA plasma. Of course, the higher the CO_2 conversion, the more CO and O_2 are produced, and the more we can expect these levels to have an influence on the results.

The vibrationally and electronically excited levels of CO_2 , CO, O_2 and N_2 , which are typically included in these models, are indicated in Table 1 with the symbols "V" and "E". Details about these notations can be found in [75,113]. For the N_2 electronically excited levels, the detailed notations are given in Table 1. Note that vibrationally excited levels might also be important for the CH_4 , H_2O and H_2 molecules, when modelling the CO_2/CH_4 , $\text{CO}_2/\text{H}_2\text{O}$, CO_2/H_2 and CH_4/O_2 mixtures in a MW or GA plasma, but to our knowledge, such models have not yet been developed in literature, and these mixtures have only been described up to now for a DBD plasma, where the vibrational levels are considered to be of minor importance [121]. For this reason, and to avoid a major complexity in the

chemical description, no vibrational levels of CH₄, H₂O or H₂ were included up to now in the existing models in literature, and the CO₂, CO and O₂ vibrational levels were also disregarded in these mixtures in a DBD plasma, to reduce the complexity and calculation time. However, a variety of higher order hydrocarbons and oxygenates were included in these models, to elucidate whether such value-added chemicals can be formed in these gas mixtures. The exact list of plasma species included in each of the models, can slightly differ among the various models, and the same is true for their chemical reactions (i.e., electron-neutral, electron-ion, ion-ion, ion-neutral and neutral-neutral reactions) and the corresponding rate coefficients. Details about these chemical reactions can for instance be found in the references cited above.

Table 1: Overview of the species typically included in plasma chemistry models for pure CO₂, pure CH₄, as well as extra species included in CO₂/CH₄, CO₂/H₂O, CO₂/H₂ and CH₄/O₂ gas mixtures, and in CO₂/N₂ or CH₄/N₂ mixtures.

Molecules	Charged species	Radicals	Excited species
Species of interest in pure CO₂ models			
CO ₂ , CO	CO ₂ ⁺ , CO ₄ ⁺ , CO ⁺ , C ₂ O ₂ ⁺ , C ₂ O ₃ ⁺ , C ₂ O ₄ ⁺ , C ₂ ⁺ , C ⁺ , CO ₃ ⁻ , CO ₄ ⁻	C ₂ O, C, C ₂	CO ₂ (Va, Vb, Vc, Vd), CO ₂ (V1-V21), CO ₂ (E1, E2), CO(V1-V10), CO(E1-E4)
O ₂ , O ₃	O ⁺ , O ₂ ⁺ , O ₄ ⁺ , O ⁻ , O ₂ ⁻ , O ₃ ⁻ , O ₄ ⁻	O	O ₂ (V1-V4), O ₂ (E1-E2)
	Electrons		
Species of interest in pure CH₄ models			
CH ₄	CH ₅ ⁺ , CH ₄ ⁺ , CH ₃ ⁺ , CH ₂ ⁺ , CH ⁺ , C ⁺	CH ₃ , CH ₂ , CH, C	CH ₄ [*]
C ₂ H ₆ , C ₂ H ₄ , C ₂ H ₂ , C ₂	C ₂ H ₆ ⁺ , C ₂ H ₅ ⁺ , C ₂ H ₄ ⁺ , C ₂ H ₃ ⁺ , C ₂ H ₂ ⁺ , C ₂ H ⁺ , C ₂ ⁺	C ₂ H ₅ , C ₂ H ₃ , C ₂ H	C ₂ H ₆ [*] , C ₂ H ₄ [*] , C ₂ H ₂ [*]
C ₃ H ₈ , C ₃ H ₆ , C ₄ H ₂		C ₃ H ₇ , C ₃ H ₅	C ₃ H ₈ [*]
H ₂	H ₃ ⁺ , H ₂ ⁺ , H ⁺ , H ⁻	H	H ₂ [*]
Extra species typically included in CO₂/CH₄, CO₂/H₂O, CO₂/H₂ or CH₄/O₂ models			
H ₂ O, H ₂ O ₂	H ₃ O ⁺ , H ₂ O ⁺ , OH ⁺ , OH ⁻	OH, HO ₂	H ₂ O [*]
CH ₂ O, CH ₃ OH, CH ₃ OOH		CHO, CH ₂ OH, CH ₃ O, CH ₃ O ₂	
C ₂ H ₅ OH, C ₂ H ₅ OOH, CH ₃ CHO, CH ₂ CO		CHCO, CH ₃ CO, CH ₂ CHO, C ₂ H ₅ O, C ₂ H ₅ O ₂	
Extra species typically included in CO₂/N₂ and/or CH₄/N₂ models			

N_2	N^+, N_2^+, N_3^+, N_4^+	N	$N_2(V1-V14), N_2(C^3\Pi_u),$ $N_2(A^3\Sigma_u^+), N_2(a'^1\Sigma_u^-),$ $N_2(B^3\Pi_g), N(2D), N(2P)$
$N_2O, N_2O_3,$ N_2O_4, N_2O_5	$NO^+, N_2O^+, NO_2^+, NO^-, N_2O^-,$ $NO_2^-, NO_3^-, N_2O_2^+$	NO, NO ₂ , NO ₃ ,	
HCN, ONCN, C ₂ N ₂	HCN ⁺	H ₂ CN, CN, NCO, NCN	
NH ₃	NH ₄ ⁺ , NH ₃ ⁺ , NH ₂ ⁺ , NH ⁺	NH ₂ , NH	NH ₃ [*]
N ₂ H ₄ , N ₂ H ₂		N ₂ H ₃ , N ₂ H	

The above balance equations for all the species densities only account for time-variations, thus neglecting spatial variations due to transport in the plasma (e.g. diffusion). Nevertheless, spatial variations in the plasma can also be included in such OD models, by imposing a certain input power or gas temperature as a function of time. In this way, we can for instance account for the occurrence of microdischarge filaments in a DBD reactor, through which the gas molecules will pass when flowing through the reactor, by applying a number of pulses as a function of time. This is for instance illustrated in [74,101,122]. Likewise, the power deposition in a MW plasma is at maximum at the position of the waveguide, which can also be accounted for, by means of a temporal profile. Indeed, we can translate the time-variation into a spatial variation in the reactor, by means of the gas flow rate. In other words, the plasma reactors are considered as a plug flow reactor, where the plasma characteristics vary as a function of distance travelled by the gas, in the same way as they would vary in time in a batch reactor. The time in the balance equations thus corresponds to a residence time of the gas in the reactor.

Next to the species densities, a OD plasma chemistry model typically also calculates the average electron energy by means of an energy balance equation, again with energy source and loss terms, defined by the power deposition (or electric field) and the chemical reactions. From the average electron energy, the energy-dependent rate coefficients of the electron processes can then be determined, while the rate coefficients of the chemical reactions between the neutral species or ions are typically adopted from literature.

In our OD models, the balance equations for the species densities are coupled to the solution of the Boltzmann equation (Bolsig+), which calculates the electron energy distribution function (EEDF) and the rate coefficients of all electron impact reactions as a function of the electron energy. However, the Bolsig+ code is not called during every time-step, so the EEDF is not updated during every time-step, but only when certain plasma quantities (e.g., the gas temperature, the reduced electric field, the electron number density or any other species number density, as defined by the user) have changed by more than a certain factor, as defined by the user. A more detailed description of the free electron kinetics in CO₂ plasma is provided in [78-83], where a state-to-state vibrational kinetic model was self-consistently coupled with the time-dependent electron Boltzmann equation. Note that when the EEDF is calculated with a Boltzmann solver, there is, strictly speaking, no need to solve the electron energy balance equation as well, because the electron impact rate coefficients can also be directly adopted from the Boltzmann solver

when cross section data is available, and the electron temperature is obtained from $T_e = \frac{2}{3} \epsilon_e$, where ϵ_e is the mean electron energy.

From the calculated plasma species densities at the beginning and the end of the simulations, corresponding to the inlet and outlet of the plasma reactor, the gas conversion, the product yields and selectivities can be obtained from the 0D models. Furthermore, based on the power introduced in the plasma and the gas flow rate, the specific energy input (SEI) can be computed, and from the latter, the energy efficiency (η) can be obtained with the following formulas:

$$SEI \left(\frac{kJ}{l} \right) = \frac{\text{Plasma power (kW)}}{\text{Flow rate} \left(\frac{l}{min} \right)} * 60 \left(\frac{s}{min} \right)$$

$$\eta(\%) = \frac{\Delta H_R \left(\frac{kJ}{mol} \right) * X_{CO_2}(\%)}{SEI \left(\frac{kJ}{l} \right) * 22.4 \left(\frac{l}{mol} \right)}$$

where ΔH_R is the reaction enthalpy of the reaction under study (e.g., 279.8 kJ/mol for CO₂ splitting) and X_{CO_2} is the CO₂ conversion. Note that the latter formula is applicable to pure CO₂ splitting. A very similar formula is applied to the other gas mixtures as well, but using another reaction enthalpy and accounting not only for the CO₂ conversion, but also for the conversion of the other gas(es) in the mixture.

The SEI can be expressed in kJ/l, as indicated in the above formula, but it is also often expressed in J/cm³ (1 kJ/l = 1 J/cm³), or in eV/molec, using the following conversion (at atmospheric pressure and room temperature):

$$SEI \left(\frac{eV}{molec} \right) = \frac{SEI \left(\frac{J}{cm^3} \right)}{2.446 \cdot 10^{19} \left(\frac{molecule}{cm^3} \right) \cdot 1.602 \cdot 10^{-19} \left(\frac{J}{eV} \right)} = SEI \left(\frac{J}{cm^3} \right) * 0.25$$

2.2. 2D or 3D fluid modeling

Although 0D chemical kinetics models are the most suitable approach for describing the detailed plasma chemistry, and some spatial dependences of the plasma reactors can be taken into account as explained above, they cannot really account for details in the reactor configuration, nor predict how modifications to the reactor geometry would give rise to better CO₂ conversion and energy efficiency. For this purpose, 2D or even 3D models are required.

As mentioned in the introduction, to our knowledge, there exist no 2D or 3D models yet for CO₂ conversion, because of the extensive computational cost, but some 2D and even 3D fluid models exist in literature, mostly for helium or argon and with simplified chemistry, for the reactors of interest for CO₂ conversion. In recent years, we also developed such fluid models in helium or argon, as they already give some insight in the effect of reactor design on the gas flow behavior and plasma characteristics. It is our purpose, however, to extend these models to CO₂, and its mixtures with the other gases mentioned above. In this paper, we show some characteristic results of these plasma reactor modeling efforts, in argon or helium, as well as first results when extending such models to CO₂. In the following paragraphs, we give some more detail on the fluid models that we developed for a packed bed DBD, MW and GA plasma.

The fluid models used to describe the plasma behavior in these reactors consist of solving conservation equations for the densities of the various plasma species and for the average electron energy. The energy of the other plasma species is assumed to be in thermal equilibrium with the gas. The conservation

equations for the species densities are again based on source and loss terms, defined by the chemical reactions, like in the 0D models. The source of the electron energy is due to heating by the electric field, and the energy loss is again dictated by collisions. In addition, transport is now also included in the conservation equations. It is defined by diffusion and by migration in the electric field (for the charged species). Furthermore, in the MW and GA plasma reactors, transport by convection due to the gas velocity (see below) is taken into account as well.

These conservation equations are coupled with the Poisson equation for a self-consistent calculation of the electric field distribution from the charged species densities. Moreover, for the GA reactor, we have also developed a more simplified quasi-neutral (QN) model, as described below, in order to further reduce the calculation time.

Finally, in the MW and GA models, the gas temperature and the gas flow behavior are calculated with a heat transfer equation and the Navier-Stokes equations, and in the GA model, the cathode heat balance is also accounted for in the axisymmetric model, to properly describe the electron emission processes, which are very important for an accurate description of the arc gliding process, as explained in section 3.2 below. The fluid (plasma) model and the models for gas flow and gas heating are combined into a multiphysics model, where the calculated gas velocity is inserted in the transport equations of the plasma species, and the gas temperature determines the gas density profile, and thus the chemical reaction rates.

These models are being developed with the COMSOL Multiphysics Simulation Software. The specific features of the models for the packed bed DBD, MW and GA plasma reactors are described below.

(a) Packed bed DBD reactor

A packed bed DBD reactor should in principle be described in 3D, to fully account for the packing geometry. However, due to very fine mesh requirements, which are inherent to the packing geometry, the calculation time in 3D, even with a simple chemistry, would be over a few months with today's computational powers. Therefore, in order to approach the 3D geometry, we have developed two different complementary axisymmetric 2D fluid models, based on a 3D unit cell of a close-packed DBD reactor, i.e., a so-called "contact point" model and a "channel of voids" model; see Figure 1 [44]. Indeed, the combination of these two models allows to describe the two important features of a packed bed plasma reactor, i.e., the contact between the beads, which enhances the local electric field in the discharge due to polarization effects, and the fact that the voids between the beads are connected, allowing the plasma to travel from one side of the discharge gap to the other. The first model accounts for two packing beads, which are slightly larger than in the real (3D) geometry, to allow them to be in direct contact with each other, while the second model describes three packing beads, with the same size as in reality, with a "channel of voids" in between them. The packing beads are treated as solid objects in the model, with zero space charge and certain dielectric properties inside the beads and charge accumulation on their surface. These models were developed in helium, (i) because of the simplified plasma chemistry, thus reducing the calculation time, and (ii) because helium yields a homogeneous discharge in a DBD, which is easier to describe with a fluid model. Details about both models and their geometries can be found in [44].

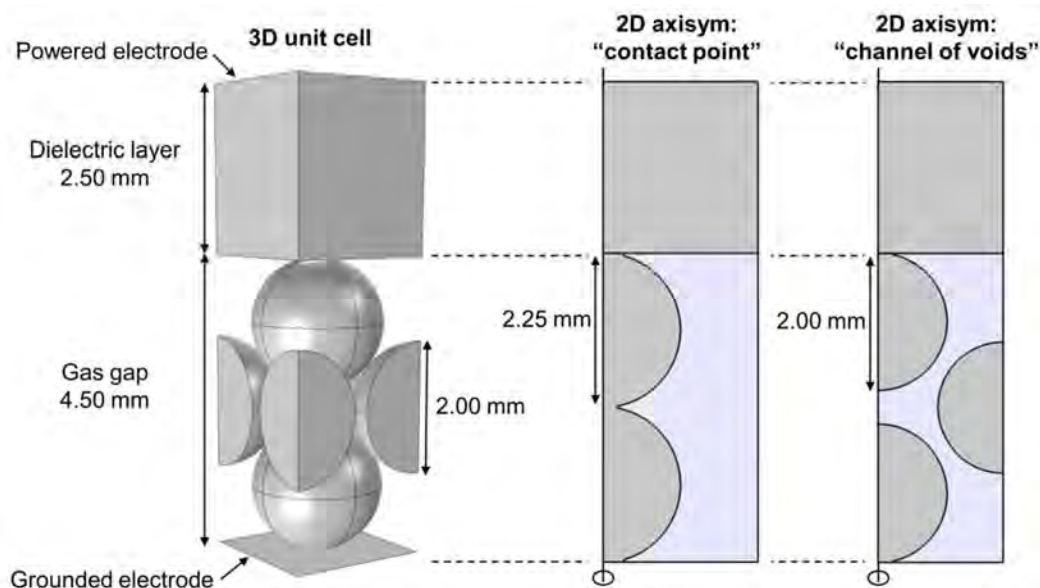


Figure 1: 3D unit cell of a packed bed DBD reactor (left) and its 2D representations used in the “contact point” model and “channel of voids” model (right). Reproduced from [44] with permission.

(b) MW plasma reactor

This model is developed for a MW surfaguide discharge used for CO₂ conversion [21,123]. The plasma tube is a cylinder, but the MW power is inserted from the waveguide at one side, so that the cylindrical symmetry is lost. However, we calculated the electromagnetic field distribution, based on the Maxwell equations, both in a 3D geometry and in a 2D axisymmetric geometry, and the results were the same, indicating that a 2D geometry gives a reasonable approximation of the MW plasma reactor. A schematic diagram of the 2D axisymmetric computational domain is depicted in Figure 2. We aim to develop this model for a CO₂ MW plasma, but we started to develop it for argon, to limit the calculation time. Details about the model and the exact equations solved can be found in [46].

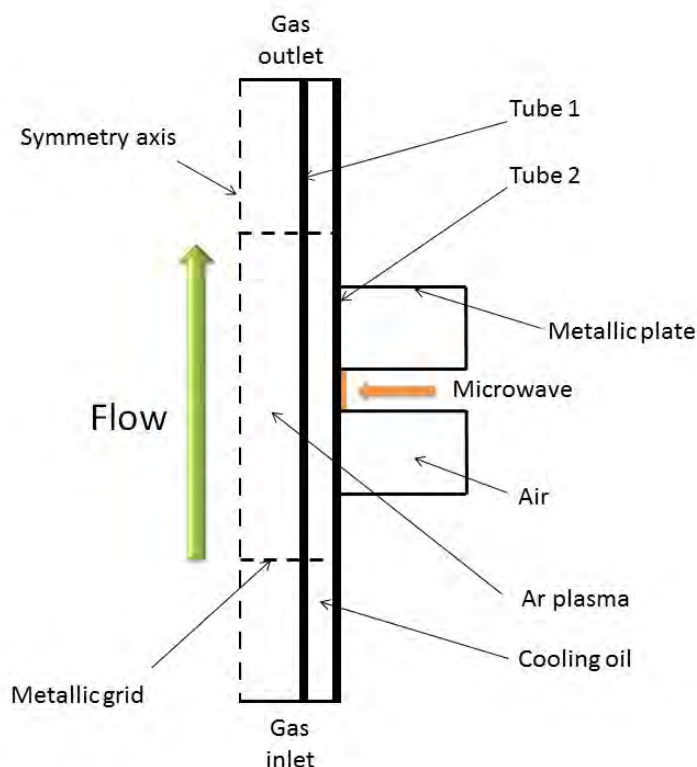


Figure 2: Schematic diagram of the MW surfaguide discharge, assumed in the model, based on the setup used in [21,123].

(c) Classical GA plasma

A classical GA plasma is an auto-oscillating periodic discharge between two diverging, flat electrodes. When applying a potential difference between both electrodes, an arc plasma is formed at the narrowest gap, which is dragged by the gas flow towards rising interelectrode distance, until it extinguishes. At that moment the discharge reignites itself at the shortest distance to start a new cycle.

The GA thus also has an intrinsically 3D nature, but again due to computational limitations, we started the model development in 2D. To be more specific, we developed again two types of 2D models, as illustrated in Figure 3, i.e., (i) a 2D axisymmetric model between two circular plates (Figure 3(a)), considering a stationary, non-gliding arc, but allowing to investigate cathode heating (if important), as well as cathode electron emission, and (ii) a 2D Cartesian model, to study the gliding arc mechanism, including arc cooling due to arc extension as a result of the gas flow and the interaction between consecutive arcs (Figure 3(b)). The latter model assumes the exact shape and size of the electrodes, taken from an experimental geometry [124], but assumes that they are infinite in the z -direction. Thus, the arc created in this model does not have a quasi-cylindrical shape, as in reality, but it is an infinite slab. Again, the combination of both models allows to study the basic mechanisms of a GA plasma. These models are also in first instance developed in argon. More details about the geometries, the equations to be solved and the approximations made in the model, can be found in [59,60].

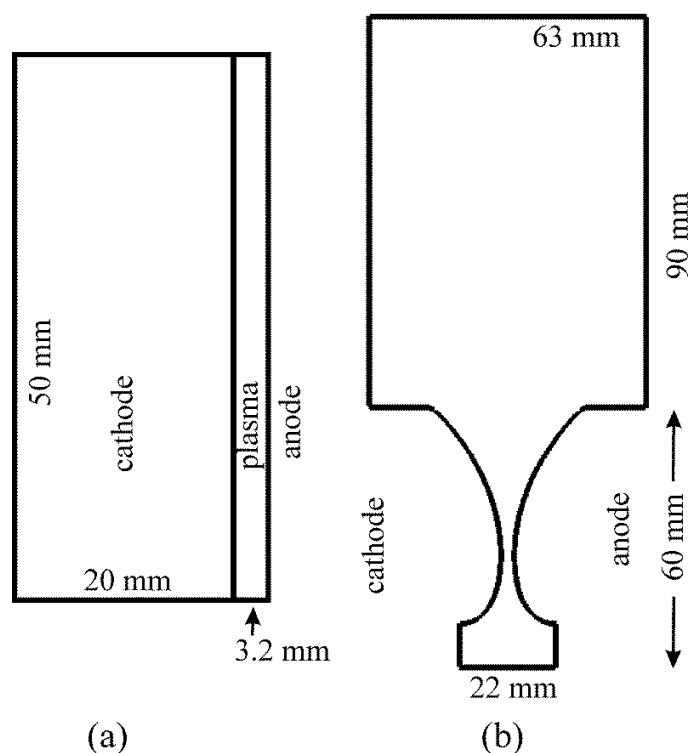


Figure 3: Geometries considered in the 2D models for the classical GA plasma: (a) 2D axisymmetric model, and (b) 2D Cartesian model.

The above model is quite time-consuming, even in 2D and with a simple argon chemistry set. Indeed, it typically runs for two weeks for a single arc cycle with the current computational power. In order to be able to apply it in 3D, and to extend it to the description of CO_2 conversion, we also developed a quasi-neutral (QN) model, as mentioned above, again for the same 2D geometries depicted in Figure 3 [61]. This QN model neglects the near-electrode regions and treats only the quasi-neutral bulk plasma. It does not solve the Poisson equation, but calculates the ambipolar electric field from the ion densities and the electron and ion diffusion coefficients and mobilities. As a result, its calculation time is a factor 5 lower than for the full, self-consistent fluid model. We compared the electron and ion densities, the gas temperature and the electric potential distributions, calculated with both the QN model and the full model, and the results are in quite good agreement, which justifies the use of this QN model for studying the gliding arc column characteristics, when no particular focus needs to be paid to the near-electrode regions [61].

This QN model was fully coupled with the gas flow model, and extended to 3D [62]. As the QN model in 3D is still very time-consuming, it can only be calculated for a very short time, in the order of 0.2 ms, within a reasonable calculation time (order of three days). However, it served to validate the fully coupled 2D QN model [62].

Furthermore, this QN model was recently also extended to CO_2 . A detailed chemical reaction set was applied, based on the full chemistry set developed in [75,76] (see Table 1 above), but somewhat reduced to account only for the most important species and reactions. In total, 5 different neutral ground state species, 2 different types of positive ions, 3 different types of negative ions and the electrons are included, as well as all the CO_2 vibrational levels, listed in Table 1 above, 3 O_2 vibrational levels and 1 CO_2 electronic level. Details of the species included in the model, as well as their corresponding reactions, can be found

in [65]. To keep the calculation time reasonable, this model was in first instance developed in 1D, considering only the radial direction of the quasi-cylindrical arc discharge channel, i.e., a transverse cross section of the plasma string along the symmetry plane of the reactor, and excluding the longitudinal direction of the plasma column [65]. However, the loss of plasma species and heat in this simulation domain, as a result of (i) the difference between the gas velocity and the gliding arc velocity, and (ii) the elongation of the arc in a real (3D) geometry due to the diverging electrodes (see Figure 3(b) above), was represented as a dilution of the arc by the incoming background gas, and it was accounted for by means of a so-called characteristic frequency of convective cooling, as explained in detail in [60,65].

As this chemistry set is still too extensive for a 2D model, we have further reduced it by lumping the 21 vibrational levels of the asymmetric stretch vibrational mode of CO₂ into a number of groups, based on the method developed in [85] (see also section 3.2 below). The lumped models with either 1, 2 or 3 groups are able to reproduce the gliding arc characteristics (i.e., gas temperature, electron temperature and electron density, as well as the CO₂ conversion) very well, but only the 3-groups model can also reproduce the characteristic shape of the vibrational distribution function (VDF), as illustrated in [64]. The reason why the lumped models with 1 and 2 groups can also reproduce the CO₂ conversion in the case studied in [65], in spite of the fact that they cannot reproduce the VDF, is because the tail of the VDF does not affect the CO₂ conversion very much when the plasma becomes too thermal (high gas temperature). Indeed, at these conditions, only the first vibrational levels are important for the conversion, since there is no significant overpopulation of the highly excited vibrational levels. On the other hand, in case of strong non-equilibrium, the shape of the VDF significantly affects the CO₂ conversion, because the highly excited levels have a very high probability of dissociation. The shape of the VDF does not significantly influence the other quantities (i.e., gas temperature, electron temperature and electron density), even in case of strong non-equilibrium, because the population of the highly excited vibrational levels is always much lower than the population of the first levels at the conditions under study here. For these quantities, it is, however, very important that the calculation is fully self-consistent and that the energy is conserved.

More details about the lumping method will be given in section 3.2 below. This level-lumping strategy opens perspectives for modeling CO₂ conversion in a GA (or MW) plasma by means of a 2D model.

(d) Reverse vortex flow GA plasma

A classical GA plasma, as described above, exhibits some disadvantages. Indeed, the flat 2D electrode geometry makes it less compatible with industrial systems, and the gas conversion is non-uniform because a considerable fraction of the gas does not pass through the active plasma region. Moreover, a high gas flow rate is needed to drag the arc, so the gas residence time is limited, which will limit the gas conversion. To overcome these drawbacks, a 3D cylindrical GA plasma reactor has been developed, based on reverse vortex flow stabilization [25,27]. The gas flows in the reactor through a tangential inlet and follows a vortex movement along the walls. An arc is again formed between both electrodes, and dragged with the tangential gas flow, thereby expanding until it extinguishes, followed by a new cycle. The vortex motion of the gas creates an isolating and cooling effect, and when it reaches one end of the reactor (closed), it continues its movement in the other direction, but with a smaller vortex (due to loss of inertia) until it leaves the reactor at the other end, where the outlet is located. Hence, this reverse vortex gas flow mixes with the arc plasma, which will be concentrated in the center. This characteristic feature seems to result in a more energy-efficient CO₂ conversion [27,33].

To properly account for the vortex flow and gliding arc behavior, this reverse vortex flow GA reactor must be described with a 3D model. To limit the calculation time, we have applied the QN model, as mentioned in previous section. The gas flow is modeled with the so-called k - ϵ Reynolds-averaged Navier-Stokes (RANS) turbulent model. A schematic picture of the reactor is illustrated in Figure 4. There are four

tangential inlets in this setup. Details about the reactor geometry, equations solved, assumptions and boundary conditions of the model, can be found in [63].

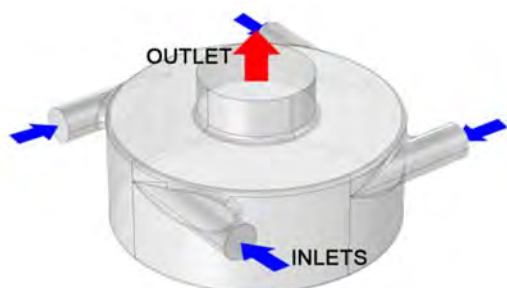


Figure 4: Schematic diagram of the reverse vortex flow GA reactor, illustrating the four inlets and the outlet. The radius of the reactor is 6.35 mm; the radius of the outlet is 2 mm; the reactor height is 5 mm.

3. Results and discussion

3.1. 0D chemical kinetics modeling

As mentioned, chemical kinetics modeling is most suitable for elucidating the underlying chemistry of the conversion process, i.e., which pathways are important for which conditions and in which type of plasma. This will be illustrated below, mainly based on our own modeling results, complemented with some results from literature, for the different gas (mixtures) of interest, i.e., pure CO₂ splitting, pure CH₄ conversion, as well as CO₂/CH₄, CH₄/O₂, CO₂/H₂ and CO₂/H₂O mixtures. More details about the modeling results in these mixtures, including the calculated conversions, product yields and energy efficiencies, and comparison with experimental data, can be found in the original research papers mentioned below, as well as in another recent review paper [125] and will thus not be repeated here. Indeed, in this paper, we will mainly focus on the reaction pathways in these gas mixtures, and how these reaction pathways can explain differences in energy efficiency for the different reactor types. However, we will show some more detailed calculation results for a CO₂/H₂O DBD plasma, as well as on mixtures of CO₂ or CH₄ with N₂, in terms of conversion, energy efficiency and product formation, as these case studies were not included in [125], and they allow us to demonstrate what type of (other) information can be obtained from the models, and how plasma chemical modeling can give more information on the underlying reaction pathways, which might help to solve specific problems.

(a) Pure CO₂ splitting

(i) DBD conditions

Figure 5 illustrates the dominant reaction pathways for CO₂ splitting in a DBD plasma, as predicted from the model in [16]. A DBD is characterized by relatively high reduced electric field values (i.e., typically above 200 Td), and thus relatively high electron energies (several eV), and for this reason, electron impact reactions with CO₂ ground state molecules dominate the chemistry. This includes electron impact dissociation into CO and O (which proceeds through an electronically excited level of CO₂, i.e., so-called electron impact excitation-dissociation), electron impact ionization into CO₂⁺ (which recombines with electrons or O₂⁻ ions into CO and O and/or O₂), and electron dissociative attachment into CO and O⁻ (see the thick black arrow lines in the reaction scheme of Figure 5). Electron impact excitation-dissociation,

ionization and dissociative attachment contribute for about 50%, 25% and 25%, respectively, to the total CO_2 conversion [74]. Because these processes require more energy than strictly needed for breaking of the C=O bond (i.e., 5.5 eV), the energy efficiency for CO_2 splitting in a DBD reactor is predicted to be quite limited, i.e., up to maximum 10 % for a conversion up to 30 %, as also observed experimentally (see Introduction).

The created CO molecules are relatively stable, but at long enough residence time, they can recombine with O^- ions or O atoms, to form again CO_2 (see thin black arrow lines in Figure 5). These backward reactions explain why the CO_2 conversion typically tends to saturate at long enough residence times (corresponding to low gas flow rates). On the other hand, the O atoms also recombine quickly into O_2 or O_3 . There are several reactions possible between O, O_2 and O_3 , also involving the O^- and O_2^- ions, as indicated by the blue arrow lines in Figure 5, and this will affect the balance between the formation of O_2 and O_3 as stable products, as explained in detail in [16].

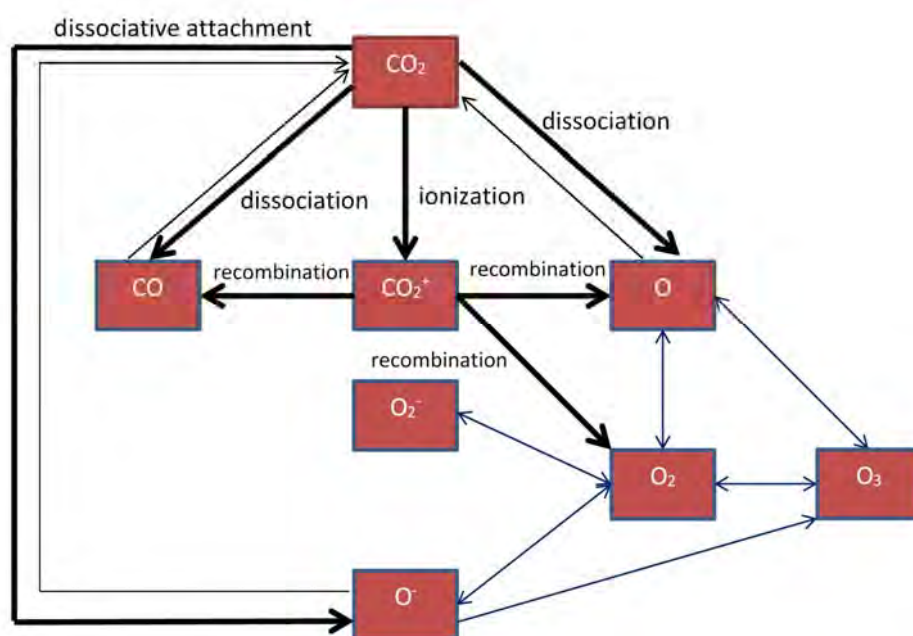


Figure 5: Dominant reaction pathways of CO_2 splitting and the further reactions between O, O_2 and O_3 in a DBD plasma, as obtained from the model in [16]. The thick black arrow lines represent the most important reactions for CO_2 splitting (mostly attributed to electron impact collisions). The thin black arrow lines point towards the opposite reactions, i.e., recombination of CO with either O^- or O, into CO_2 . The blue arrow lines indicate the conversions between O, O_2 and O_3 .

A crucial aspect in plasma chemistry modeling, in general, is the accuracy of the input data, like cross sections and rate coefficients. This is also true for modeling the plasma chemistry of CO_2 conversion. More specifically, there is some confusion in literature about the most accurate cross section for CO_2 dissociation, as the latter process is believed to proceed through electron impact excitation, as mentioned above, but it is not clear from literature which excitation channels effectively lead to dissociation. The various cross sections are discussed in detail in a recent paper [125]. Pietanza et al. performed a parametric evaluation, for a wide range of reduced electric fields and vibrational temperatures, to

compare the calculated EEDF and the CO_2 dissociation rates in pure CO_2 plasmas, using two different electron impact excitation-dissociation cross sections, more specifically, the data from Phelps [127-129] with a threshold of 7 eV, and the ones of Cosby and Helm [130], with a threshold of 12 eV. They reported differences up to orders of magnitude, depending on the reduced electric field assumed, and they advised to use the excitation cross section with threshold of 7 eV reported by Phelps as the dissociation channel, while considering the process with threshold of 10.5 eV as normal electronic excitation [78-80].

Ponduri et al. [77] developed a 1D fluid model, based on a very similar plasma chemistry as developed in our group [74-76] to model CO_2 conversion in a DBD. When assuming only electron impact dissociation based on Itikawa's cross section [131], their calculated CO_2 conversion was about one order of magnitude lower than experimental values, obtained in a wide range of specific energy input (SEI), as illustrated in Figure 6. On the other hand, when also including the excitation cross sections with thresholds of 7 eV and 10.5 eV reported by Phelps for the dissociation process, their calculated CO_2 conversion was too high. Finally, when only including the dissociation cross section of Itikawa and the excitation cross section with the 7 eV threshold for the dissociation process, a reasonable agreement with experiments was reached, although the calculated CO_2 conversion was overestimated by a factor 2 (see Figure 6).

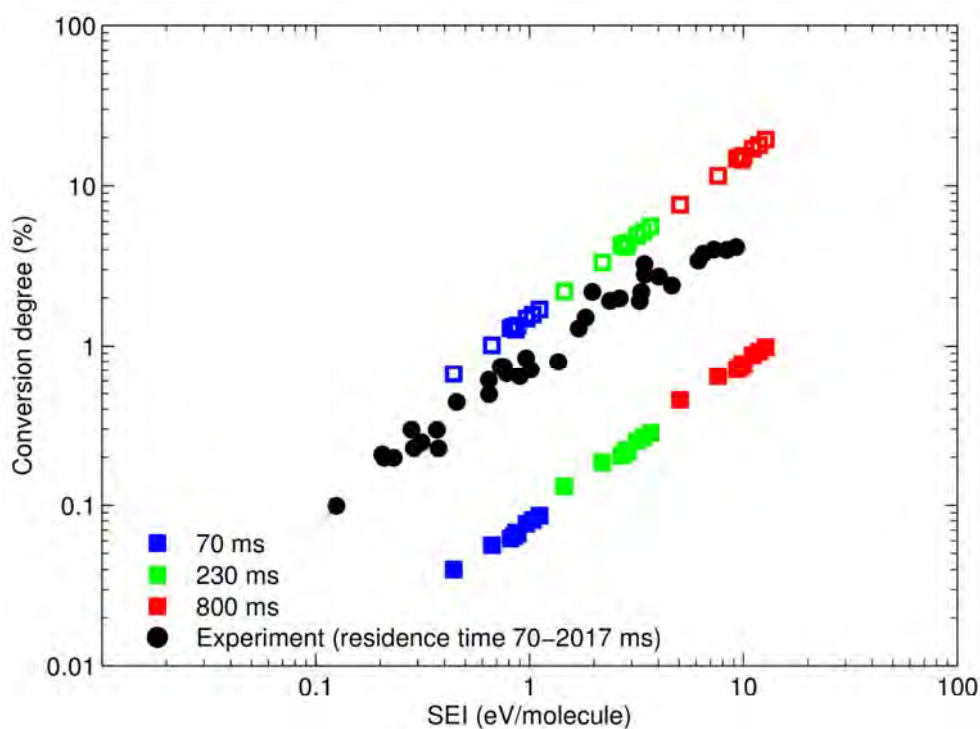


Figure 6: Calculated CO_2 conversion as a function of the specific energy input (SEI) for various residence times (70, 230 and 800 ms), as obtained from the model in [77], considering only electron impact dissociation according to the Itikawa cross section (full symbols) and also considering the Phelps cross section with threshold of 7 eV (open symbols), and comparison with experimental data of [132]. Reproduced from [77] with permission.

In [122] we also investigated the effect of various dissociation cross section on the CO_2 conversion, and we came to similar conclusions. The cross sections proposed by Itikawa [131], as well as those by Polak

and Slovetsky [133], both underestimate the CO₂ conversion, while the data reported by Phelps with threshold of 7 eV and 10.5 eV yield a CO₂ conversion only slightly lower than the experimental data, but the sum of both cross sections overestimated the values [122]. This indicates that these cross sections most probably also include other excitation channels, not leading to dissociation.

Because of the complex plasma chemistry and the uncertainties of some of the assumptions made in the models, as well as possible uncertainties in the experimental data, it is not possible to draw final conclusions on which cross section is the most realistic, but we believe that the Phelps cross section with 7 eV threshold should give rise to dissociation, as well as a certain fraction of the Phelps cross section with 10.5 eV threshold. However, more detailed investigations on the CO₂ electron impact excitation-dissociation cross sections, either through measurements or quantum chemical calculations, are crucially needed to elucidate which excitation channels exactly lead to dissociation. As long as this is not known, we propose that future modeling studies may use the Phelps 7 eV cross section, keeping in mind that it might neglect some additional dissociation channels (probably associated with the 10.5 eV threshold), and thus it might underestimate to some extent the actual CO₂ conversion.

(ii) MW and GA conditions

While at typical DBD conditions, our calculations predict that ca. 94% of the CO₂ splitting is achieved from the ground state, and only ~6% occurs from the vibrationally excited levels [74], this situation is completely different in a MW or GA plasma. Indeed, these plasma types are characterized by much lower reduced electric field values (in the order of 50-100 Td), creating lower electron energies (order of 1 eV), and thus the CO₂ splitting is mainly induced by electron impact vibrational excitation of the lowest vibrational levels, followed by vibrational-vibrational (VV) collisions, gradually populating the higher vibrational levels, leading to dissociation of CO₂. This stepwise vibrational excitation, or so-called “ladder-climbing” process, is illustrated in Figure 7. This process only requires 5.5 eV for dissociation, i.e., exactly the C=O bond energy, while the dominant process in a DBD, i.e., electron impact dissociation, requires 7-10 eV, as it proceeds through a dissociative electronically excited level of CO₂, as explained above, and as is clear from Figure 7. This “waste of energy” explains the lower energy efficiency in a DBD plasma vs a MW or GA plasma, as mentioned in the Introduction.

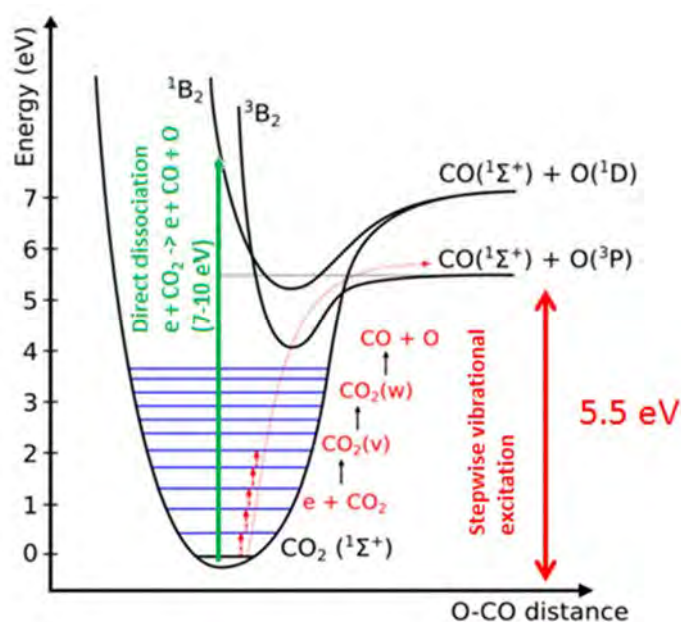
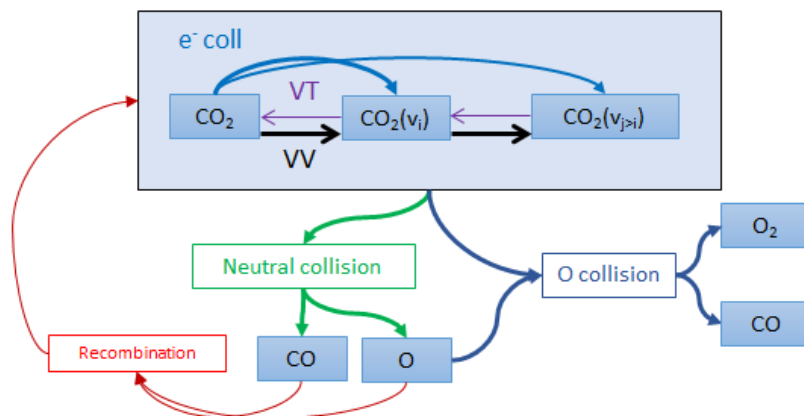


Figure 7: Schematic illustration of some CO₂ electronic and vibrational levels, illustrating the energy efficient dissociation process through electron impact vibrational excitation, followed by vibrational-vibrational collisions, which gradually populate the higher vibrational levels, i.e., so-called ladder climbing (red curve: 5.5 eV), compared to direct dissociation through electronic excitation (green arrow line: 7-10 eV).

It should, however, be mentioned that the vibrational excitation pathway is not always optimized in a MW or GA plasma. Indeed, the vibrational excitation is higher at lower pressures and higher power densities in a MW plasma, as illustrated in detail in [88]. A higher power density gives rise to higher electron densities, which yield more vibrational excitation. Higher pressures, however, result in more vibrational-translational (VT) relaxation processes, so that the vibrational energy is lost again more quickly. Also the gas temperature plays a crucial role. A higher gas temperature also results in more pronounced VT relaxation, so that the vibrational levels thermalize faster. Thus, our model predicts that in a MW plasma at high pressure (e.g., 1 atm), the dissociation is too much determined by thermal processes, thus limiting the CO₂ conversion and energy efficiency, as also experimentally observed. Furthermore, the recombination of CO and O atoms also becomes gradually more and more important at high gas temperature and pressures, as illustrated in [88], further explaining why the experimental CO₂ conversion and energy efficiency drop upon increasing pressure. The main processes occurring in the MW plasma in the two extreme cases, i.e., on the one hand the ideal non-equilibrium conditions of low pressure and temperature and high power densities, and on the other hand the near-thermal conditions of high pressure and temperature, are summarized in Figure 8. The model predicts a maximum CO₂ conversion of about 40% at an energy efficiency of 60% in a pressure range of 150-200 mbar [88], and we expect that these values could still be enhanced if the non-equilibrium conditions can be further exploited, while at atmospheric pressure, in the near-thermal conditions, the CO₂ conversion and energy efficiency drop till about 10% and 15%, respectively [88]. Hence, it is clear that we should exploit as much as possible the non-equilibrium character of a MW plasma, where the higher vibrational levels of CO₂ are overpopulated, as this is important for energy efficient CO₂ conversion. To realize this, it is thus beneficial to work at

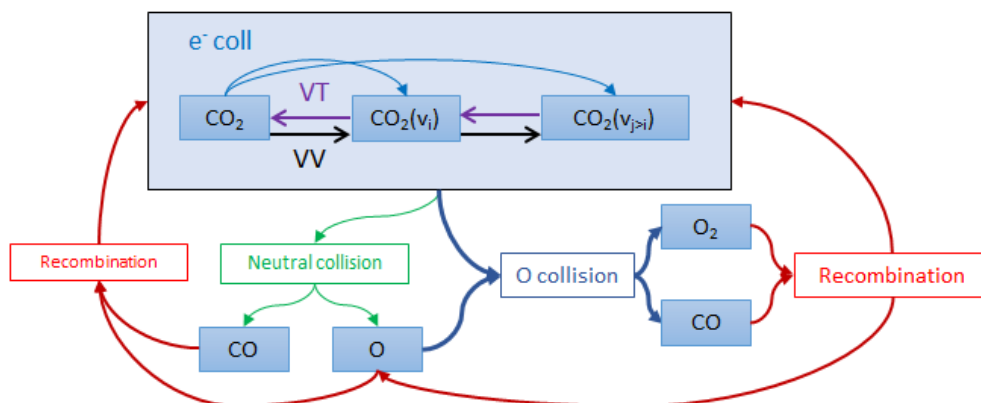
reduced pressure, and at the same time at sufficiently high power densities, while keeping the gas temperature under control [88].

a) Non-equilibrium conditions



- High vibrational excitation + VV; low VT
- Dissociation by neutral and O collisions equally important
- Low recombination
- Energy efficient

b) Near-thermal equilibrium conditions



- Thermal VDF due to high VT
- High recombination
- Energy lost to heat

Figure 8: Dominant reaction pathways of CO_2 splitting in a MW plasma, as obtained from the model in [88], for two extreme cases: (a) the ideal non-equilibrium conditions of low pressure and temperature and high power densities, and (b) the near-thermal condition of high pressure and temperature.

Likewise, also in a GA plasma, our models predict that the CO₂ conversion could be further enhanced, by exploiting more the role of the higher vibrational levels of CO₂. Indeed, the major dissociation process at typical GA conditions appears to be electron impact dissociation of the lower CO₂ vibrational levels, because the vibrational distribution function (VDF) is too much thermal, i.e., there is no significant overpopulation of the higher CO₂ vibrational levels. This was predicted both in a classical GA [64] as well as in a RVF GA, where at high temperatures (~2500 – 3000 K) the CO₂ dissociation even proceeds mainly from the ground state, as obtained by the model [33]. Indeed, the models reveal that reactions of the higher vibrational levels with heavy particles (i.e., either O atoms or any arbitrary molecules in the plasma), which would be the most energy efficient process for CO₂ conversion, are of minor importance in both the classical and RVF GA at standard conditions. Just like in the MW plasma, the model predicts that a significant overpopulation of the VDF, and thus a more energy efficient CO₂ conversion, can be realized by decreasing the temperature or by increasing the power density [64].

This is schematically illustrated in Figure 9: The predicted CO₂ conversion and energy efficiency are about 7 % and 30 % at the standard conditions of the model (i.e., assumed gas temperature inside the arc of 1200 K, power density of 3.6×10^4 W/cm³, and assuming that 20% of the gas can pass through the arc) [64], but these values can be significantly improved accordingly to the model, to a conversion of nearly 20 % and a corresponding energy efficiency up to 80-100 %, when either the gas temperature in the arc is reduced to 1000 K, or the power density rises to 4.6×10^4 W/cm³, or when the backward (recombination) reaction is removed from the model. Furthermore, if the gas fraction that can pass through the arc zone could be enhanced, for instance by inducing a difference in gas flow velocity and arc gliding velocity (see below), both the conversion and energy efficiency would also increase, provided that the larger treated gas fraction can compensate for the reduced processing time on each part of treated gases.

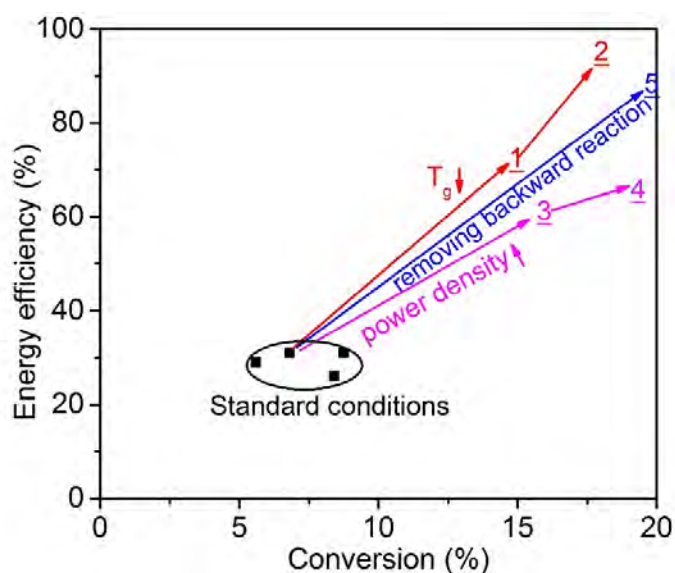


Figure 9: Energy efficiency vs CO₂ conversion in a classical GA reactor, as calculated by the model of [64] for standard conditions as assumed by the model, and improvements predicted by the model, by either reducing the gas temperature in the arc from 1200 K to 1100 K and 1000 K (no 1 and 2, at power density of 3.6×10^4 W/cm³), or increasing the power density (from 3.6×10^4 to 4.1×10^4 and 4.6×10^4 W/cm³ (no 3 and 4, at $T_g = 1200$ K) or by removing the backward (recombination) reaction from the model (no 5).

(b) Pure CH₄ reforming

Besides CO₂ splitting, CH₄ reforming into higher hydrocarbons and H₂ by means of plasma technology is also of great interest. The dominant reaction pathways in a DBD plasma, as predicted by the model in [91], are illustrated in Figure 10. Like in the case of CO₂ splitting, the CH₄ conversion is initiated by electron impact dissociation, into CH₃ radicals. The latter will recombine into higher hydrocarbons, such as C₂H₆ and C₃H₈. These hydrocarbons, as well as CH₄ itself, will also dissociate into H₂ formation. Moreover, various dissociation and recombination reactions lead to the other, unsaturated hydrocarbons. Details about the exact reaction mechanisms can be found in [91].

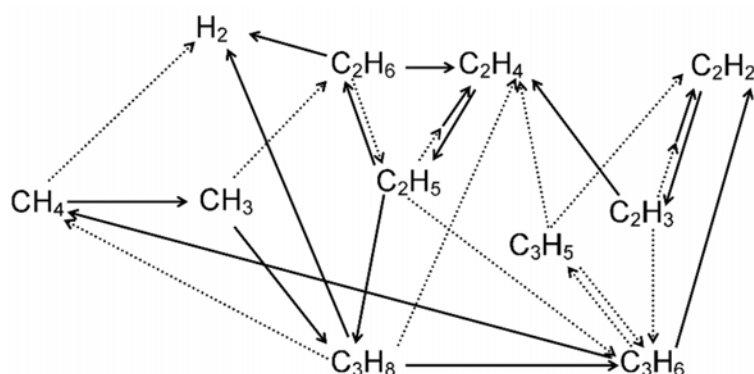


Figure 10: Dominant reaction pathways for the conversion of CH₄ into higher hydrocarbons and H₂ in a DBD plasma, as obtained from the model in [87]. The most important reactions are indicated with a solid line, while the dashed lines represent the less important reactions. Reproduced from [125] with permission.

(c) CO₂/CH₄ mixture

Combining CO₂ and CH₄ conversion in a plasma leads to the formation of H₂, CO, higher hydrocarbons and oxygenates. The dominant pathways, as predicted by the model in [104] are illustrated in Figure 11. The thickness of the lines corresponds to the “importance” of the reaction. As illustrated above, CH₄ dissociation is initiated by electron impact, forming CH₃ radicals, which recombine into higher hydrocarbons. Moreover, electron impact dissociation of CH₄ and of the higher hydrocarbons also yields H₂ formation, like in the case of the pure CH₄ plasma (see above). However, in the CO₂/CH₄ plasma, the CH₃ radicals do not only create higher hydrocarbons, but also methanol (CH₃OH) and CH₃O₂ radicals, albeit to a lower extent. Furthermore, the CH₂ radicals, also created from electron impact dissociation of CH₄, react with CO₂ to form formaldehyde (CH₂O) and CO. Finally, the O atoms, created from electron impact dissociation of CO₂ (see also Figure 5 above), also initiate the formation of higher oxygenates, like acetaldehyde (CH₃CHO), which reacts further into CH₃CO radicals, and the latter can be further converted into ketene (CH₂CO). However, these pathways are not so important in absolute terms, as indicated by the thin dashed lines in Figure 11.

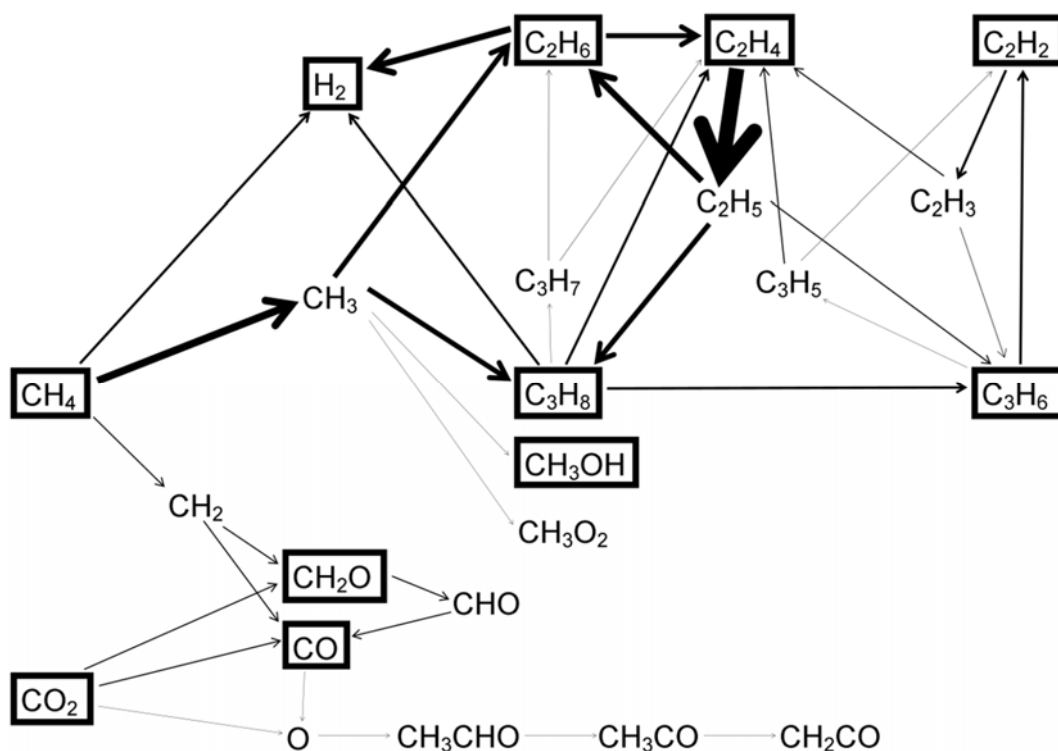


Figure 11: Dominant reaction pathways for the conversion of CH_4 and CO_2 into higher hydrocarbons, H_2 , CO and higher oxygenates, in a 70/30 CH_4/CO_2 DBD plasma, as obtained from the model in [104]. The thickness of the arrow lines corresponds to the importance of the reaction paths. Reproduced from [125] with permission.

(d) CH_4/O_2 mixture

To compare the chemistry in the CO_2/CH_4 mixture, i.e., used for dry reforming of methane, with that of partial oxidation of methane, i.e., a CH_4/O_2 mixture, we illustrate the reaction pathways of the latter mixture in Figure 12, as predicted again by the model in [104]. The thickness of the arrow lines is again correlated to the rate of the net reactions. It is quite obvious that the CH_4/O_2 mixture leads to a completely different chemistry than the CO_2/CH_4 mixture, in spite of the fact that the same chemical species are included in the models (see Table 1 above). Electron impact dissociation of CH_4 again leads to CH_3 radicals, which will recombine into methanol or higher hydrocarbons. However, the recombination into CH_3O_2 radicals, which form either CH_3O radicals or methyl hydroperoxide (CH_3OOH), is now more important. The CH_3O radicals produce methanol, which is obviously a more important formation mechanism than the recombination of CH_3 with OH radicals (cf. the arrow line thickness in Figure 12), and methanol can also react further into CH_2OH radicals, producing formaldehyde. The latter is also easily converted into CHO radicals, and further into CO (note the thickness of these arrow lines, indicating the importance of these reactions) and CO_2 . Furthermore, formaldehyde is also partially converted into H_2O . It is important to stress that this pathway is illustrated for a 70/30 CH_4/O_2 mixture, which obviously leads to nearly full oxidation of CH_4 , rather than partial oxidation, where the major end products should be the higher oxygenates. When less O_2 would be present in the mixture, our model predicts that methanol and methyl hydroperoxide are formed in nearly equal amounts as CO and H_2O [104].

As far as O_2 is concerned, it is mainly converted into CO, O atoms and HO_2 radicals, as is clear from Figure 12. Also some O_3 is formed out of O_2 , but the reverse process, i.e., the production of two O_2 molecules out of O_3 and O atoms, is more important, explaining why the arrow points from O_3 towards O_2 . The balance between O, O_2 and O_3 was also clear from Figure 5 above, and is explained in detail in [16]. Furthermore, the O atoms are converted into CH_3O and OH radicals, producing methanol and water, respectively. Especially the latter reaction (from OH to H_2O) appears to be very important, as indicated from the thick arrow line, and thus, significant amounts of H_2O are formed, as predicted by the model [104].

In summary, the comparison between Figures 11 and 12 clearly points out that the chemical pathways in a CH_4/O_2 and CH_4/CO_2 plasma are quite different, even at the same mixing ratios. Furthermore, it is clear that in both mixtures a large number of different chemical compounds can be formed, but due to the reactivity of the plasma, there is no selective production of some targeted compounds. To reach the latter, the plasma will have to be combined with a catalyst.

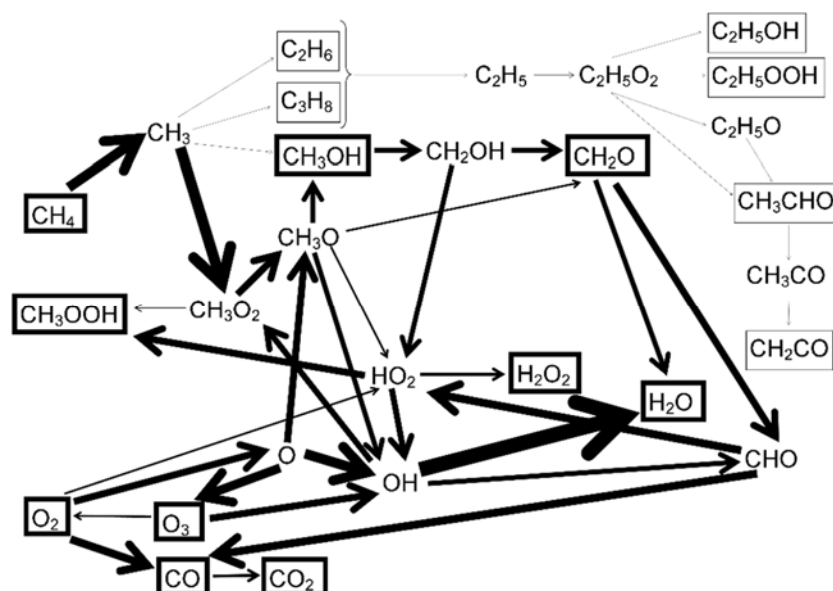


Figure 12: Dominant reaction pathways for the conversion of CH_4 and O_2 into (mainly) higher oxygenates, as well as some full oxidation products, in a 70/30 CH_4/O_2 DBD plasma, as obtained from the model in [104]. The thickness of the arrow lines corresponds to the importance of the reaction paths. Reproduced from [125] with permission.

(e) CO_2/H_2 mixture

Another possible candidate for the production of value-added chemicals from CO_2 is a CO_2/H_2 mixture. Figure 13 illustrates the dominant reaction pathways for the conversion of CO_2 and H_2 in a 50/50 CO_2/H_2 DBD plasma, as predicted by the model in [112]. Again, the thickness of the arrow lines is proportional to the rates of the net reactions. Like before, the conversion starts with electron impact dissociation of CO_2 , yielding CO and O atoms. Simultaneously, and much more pronounced, is the electron impact dissociation of H_2 , resulting in the formation of H atoms (cf. the thickness of the arrow line). The O and H atoms recombine into the formation of OH radicals, and further into H_2O . The model thus predicts that H_2O is produced at relatively high density [112], which is not an interesting product, in contrast to for instance CO.

The CO molecules will partially react back into CO₂, mainly through the formation of CHO radicals. This pathway appears to be more important than the direct three-body recombination between CO and O atoms into CO₂, which is the dominant pathway in a pure CO₂ plasma. The H atoms thus contribute significantly to the back reaction of CO into CO₂, and this explains why the CO₂ conversion is quite limited in the CO₂/H₂ mixture, as predicted by the model [112]. In addition, electron impact dissociation of CO results in the formation of C atoms, which react further into CH, CH₂, C₂HO and CH₃ radicals in several successive radical recombination reactions. The CH₂ radicals react with CO₂ into the formation of CH₂O, while the CH₃ radicals easily form CH₄. The latter appears much more favored than the formation of CH₃OH out of CH₃. CH₄ partially reacts further into higher hydrocarbons (C_xH_y).

It is thus clear from Figure 13 that several subsequent radical reactions are needed for the formation of (higher) hydrocarbons and oxygenates, such as CH₄, C₂H₆, CH₂O and CH₃OH. This explains the very low yields and selectivities of these end products, as predicted by the model [112]. In summary, the lack of direct formation of CH₂ and CH₃ in the CO₂/H₂ mixture, which is important in CO₂/CH₄ gas mixtures (see Figure 11 and [104]), combined with the very low conversion of CO₂, which is again due to the absence of CH₂ as important collision partner for the loss of CO₂, seems to make the CO₂/H₂ mixture less interesting for the formation of higher hydrocarbons and oxygenates than a CO₂/CH₄ mixture at the conditions under study. In addition, H₂ itself is a useful product, while CH₄, besides being a fuel itself, also greatly contributes to global warming, and thus, the simultaneous conversion of CO₂ and CH₄ can reduce the concentration of two greenhouse gases. Furthermore, CO₂/CH₄ mixtures are available from biomass installations, and their simultaneous conversion is thus considered to be a direct valorization of biogas. Thus, we may conclude that a CO₂/H₂ DBD plasma (at least without catalysts) might not be an optimal choice for CO₂ conversion into value-added chemicals.

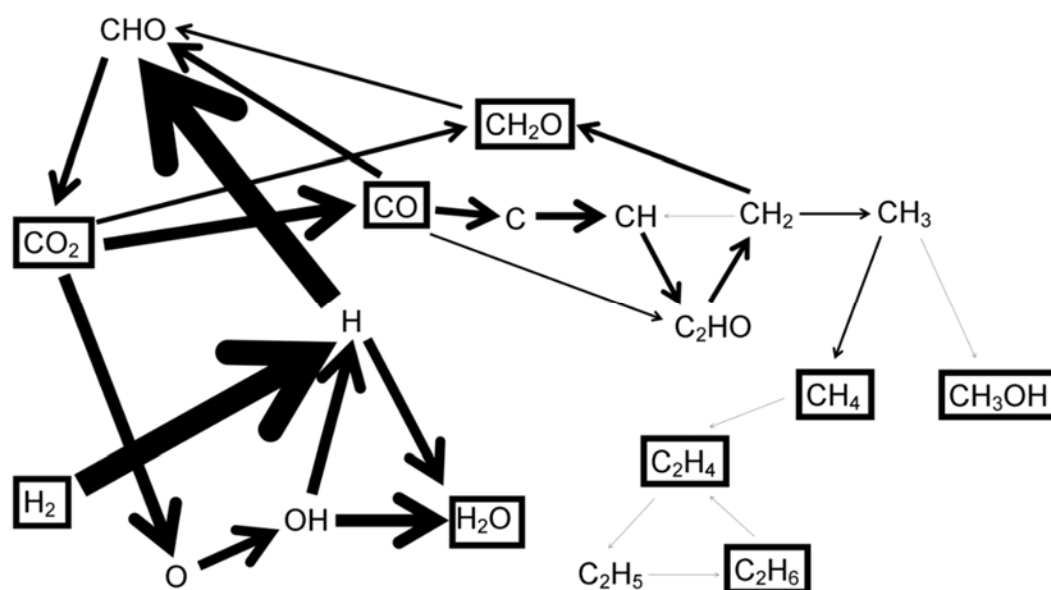


Figure 13: Dominant reaction pathways for the conversion of CO₂ and H₂ into various products, in a 50/50 CO₂/H₂ DBD plasma, as obtained from the model in [112]. The thickness of the arrow lines corresponds to the rates of the net reactions. The stable molecules are indicated with black rectangles. Reproduced from [112] with permission.

(f) CO₂/H₂O mixture

Finally, the cheapest and therefore most interesting H-source that could be added to the CO₂ plasma, in order to directly produce value-added chemicals, like oxygenated hydrocarbons or syngas (H₂/CO mixture) is H₂O. The combined conversion of CO₂ and H₂O could mimic the natural photosynthesis process. However, it was demonstrated, by means of combined modelling and experiments, that when adding H₂O (in concentrations up to 8%) to a CO₂ DBD plasma, the CO₂ conversion is reduced, and only quite low CO₂ and H₂O conversions can be obtained. More importantly however, no oxygenated hydrocarbons were detected in the experiments, and the calculated concentrations were no higher than the ppb level [111].

Because the CO₂ and H₂O conversion, the H₂/CO ratio, and the other product selectivities were in very good agreement between model calculations and experiments [111], the model was used to run simulations in a wider range of H₂O concentrations, which could not be realized in the DBD setup used in [111]. Although extreme caution is advised when extrapolating models outside their validated range, previous experience with these plasma chemistries tells us that in general most behaviors and trends can indeed be extrapolated to a somewhat wider range of conditions [102,114,120]. This allows us to investigate whether the same results can be expected in this wider range, and/or whether certain products can be formed in larger amounts, and thus, whether it would be worth pursuing these other conditions experimentally.

Figure 14 illustrates the calculated CO₂ and H₂O conversions, as well as the obtained H₂/CO ratio, as a function of the H₂O concentration in the gas mixture, for a wide range of SEI values. The CO₂ conversion increases with SEI, as expected, and it drops with increasing H₂O concentration over the entire range, although the initial drop (from 0 to 10% H₂O content) is most pronounced. This result is thus similar to the observations made in [111].

The H₂O conversion, however, shows some interesting behavior: it exhibits different trends depending on the SEI. For a low SEI of 5 and 10 J/cm³ the H₂O conversion increases with SEI and decreases with increasing H₂O content, while for an SEI of 100 and 250 J/cm³ the H₂O conversion increases upon rising H₂O content. Moreover, at the low H₂O contents, the H₂O conversion drops with increasing SEI, which is rather unexpected. The results at 25 and 50 J/cm³ show intermediate behavior.

It seems that, at low H₂O contents in the mixture and low SEI values, increasing the SEI will lead to more H₂O conversion, as expected, but only until about 25 J/cm³, while higher SEI values cause a drop in the H₂O conversion. Our model indeed reveals that an equilibrium in the chemistry is reached, where the backward reactions (i.e., the recombination of OH and H into H₂O) start to become equally important as the forward reactions (i.e., the splitting of H₂O into OH and H). This means that the conversion stops increasing and even starts decreasing upon higher SEI values.

The H₂/CO ratio, plotted in Figure 14(c), increases drastically with the H₂O content, which is like expected. Moreover, it drops with increasing SEI, as was also reported in literature [129]. This drop can be explained from Figure 14(a,b), because the CO₂ conversion keeps on increasing with SEI, while the H₂O conversion starts to saturate with increasing SEI, or it even drops with SEI at low H₂O contents. As CO is formed out of the CO₂ conversion, while H₂ is created from the H₂O conversion, it is quite logical that the H₂/CO ratio drops upon rising SEI.

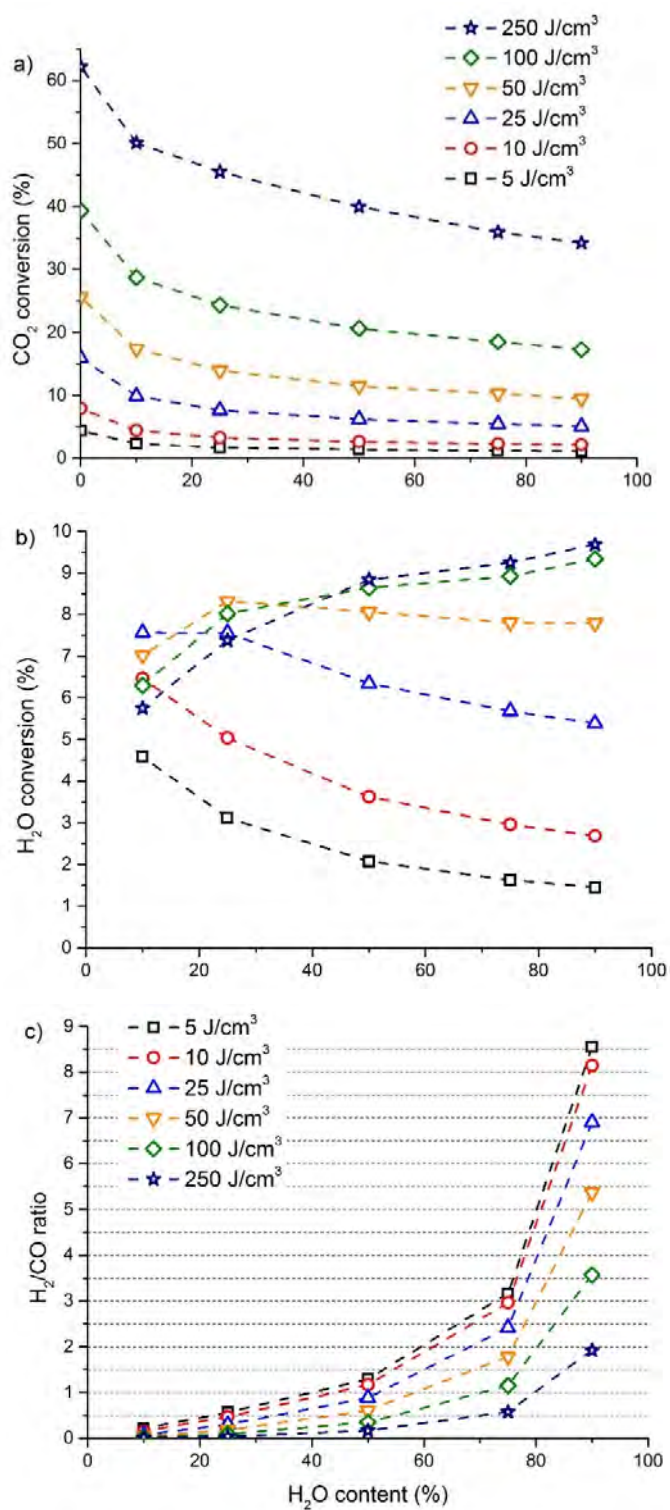


Figure 14: CO₂ (a) and H₂O (b) conversion, and H₂/CO ratio (c), as a function of H₂O content in a CO₂/H₂O DBD plasma, for different values of SEI, as obtained with the model in [111].

As illustrated in Figure 14(c), the H_2/CO ratio varies between 0.0076 (at low H_2O contents and a high SEI value of $250 J/cm^3$) and 8.6 (for the highest H_2O content of 90% and a SEI value of $5 J/cm^3$). Thus, it is clear that plasma technology allows for a process with an easily controllable H_2/CO ratio, and that the ratio can be controlled in two ways, i.e., by both the H_2O content and the SEI value. The high H_2/CO ratio obtained at high H_2O contents and low SEI values is important for applications, as this mixture might be directly used in Fischer-Tropsch synthesis for the production of liquid hydrocarbons, and it might also be suitable for methanol synthesis. Thus, even if no direct methanol (or other oxygenated hydrocarbon) formation is possible in the plasma, the H_2/CO ratio obtained might be useful for valorization purposes.

With respect to the formation of other products, our model predicts that besides the syngas components (CO and H_2), O_2 is the main product of the CO_2/H_2O mixture, as was also observed in [111], and that again no oxygenated hydrocarbons are formed, at least not in concentrations above 20 ppm. However, the production of H_2O_2 increases significantly upon rising SEI and H_2O content in the mixture, reaching concentrations between 300 ppm and 2.2 %, depending on the SEI and H_2O content.

The (O-based and H-based) selectivity of the major products is plotted in Figure 15, as a function of H_2O content and for three different SEI values. The results at an SEI of 5 and $25 J/cm^3$ are very similar (cf. Figure 15(a,b)). At $25 J/cm^3$, the O_2 selectivity increases slightly from 50 to 57 % when adding up to 50 % H_2O and then decreases slightly again to 46 %. The CO selectivity, on the other hand, exhibits a continuous drop from 48 to 9 % upon rising H_2O content, which is logical, because of the lower CO_2 content in the gas mixture. This drop in CO selectivity is balanced by the (O-based) H_2O_2 selectivity, which increases at the same time from 1 to 45 %, for H_2O contents rising from 10 to 90 %, which is again logical. The H-based selectivity for H_2O_2 also generally rises with increasing H_2O content, although the effect is not so pronounced as for the O-based selectivity, with an initial drop from 9 to 8 % (up to 25 % H_2O content), followed by a rise to 27 %. The reason that the effect is less pronounced is because the other product (H_2) also originates from the H_2O splitting. Indeed, the behavior of the H-based selectivity towards H_2O_2 is mirrored by the selectivity towards H_2 , which first increases from 91 to 92 %, followed by a drop to 73 %. At $5 J/cm^3$, the results are almost the same, with only slight differences in the absolute values.

At $250 J/cm^3$, the trends for the O-based selectivity are also similar (see Figure 15(c)), although the CO selectivity is somewhat higher and the H_2O_2 selectivity is somewhat lower than at the lower SEI values. The H-based selectivity, however, is clearly different, with an increasing H_2 selectivity and a decreasing H_2O_2 selectivity upon rising H_2O content, which is opposite to the trends observed at lower SEI values. This illustrates that the H_2O chemistry seems to undergo drastic changes with increasing SEI, due to the equilibrium reached between H_2O splitting and formation, as could also be deduced from the H_2O conversion plotted in Figure 14(b) above. At low H_2O content in the mixture, the H_2O_2 selectivity is 40%, but it drops to 25% at high H_2O contents. Combining these (O-based and H-based) H_2O_2 selectivities with the conversions of H_2O and CO_2 plotted in Figure 5 above, tells us that significant yields of H_2O_2 can be formed, up to the % range, as mentioned above.

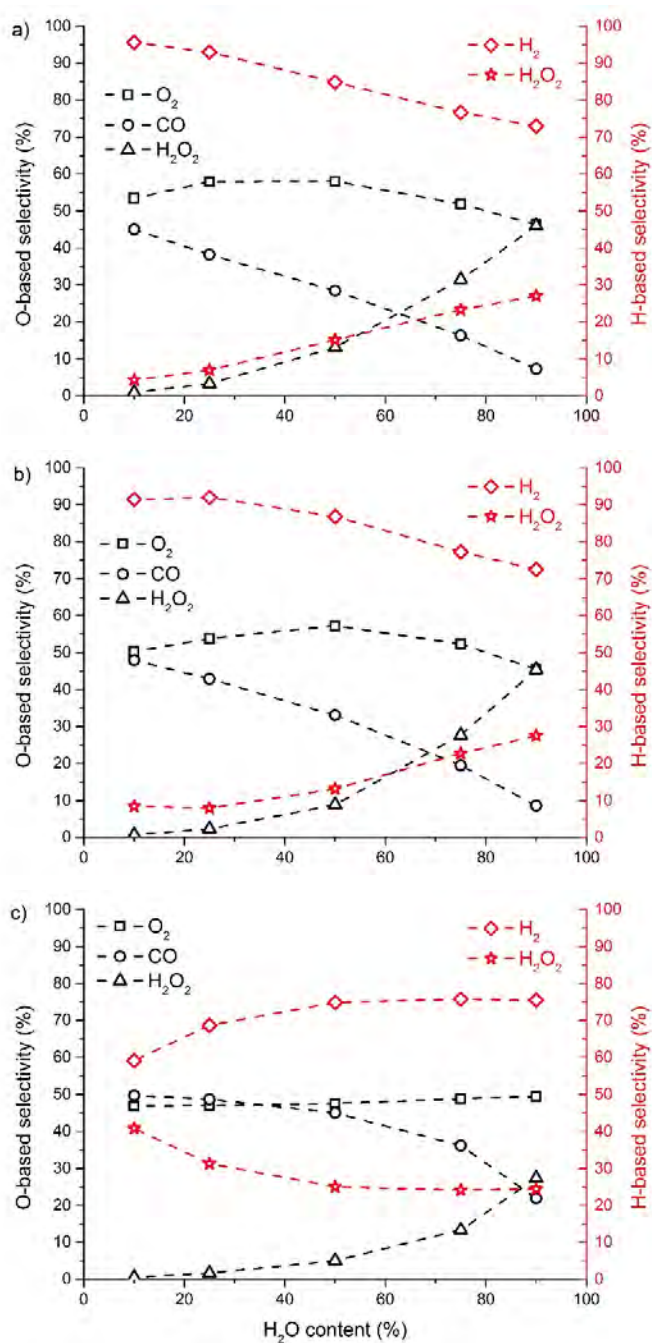


Figure 15: O-based (black symbols, left axis) and H-based (red symbols, right axis) selectivity of the major products, as a function of H₂O content in the mixture, for an SEI value of 5 J/cm³ (a), 25 J/cm³ (b) and 250 J/cm³ (c).

As good agreement was obtained between model and experiments in the range of H₂O concentrations investigated experimentally, we believe that the model gives a realistic description of the underlying chemistry. Hence, we can try to explain the trends observed here, by means of a kinetic analysis of the reaction chemistry, as revealed by the model. The model predicts that the CO radicals, formed out of CO₂ splitting, quickly react with the OH radicals, created out of H₂O splitting, yielding H atoms and CO₂.

Furthermore, these H atoms and the ones originating from H₂O splitting, react back into H₂O through a number of steps, involving O, O₂, HO₂ and OH (see details in [111]). These reactions explain why the H₂O conversion is limited to a maximum of 10% (see Figure 14(b)), because an equilibrium is reached between H₂O splitting and formation, as also mentioned above. More importantly, it also explains why the CO₂ conversion is reduced upon addition of H₂O in the mixture (see Figure 14(a)). Note that this drop in CO₂ conversion is remarkable, because in general, a rise in (absolute) CO₂ conversion is found upon addition of another gas, such as N₂ [113,114], He [6,17] or Ar [17].

Moreover, the kinetic analysis clarifies why no oxygenated hydrocarbons are formed in the CO₂/H₂O mixture. Indeed, the H atoms react with O into OH and subsequently into H₂O, as indicated above, instead of forming CH and CHO fragments, which are essential to create e.g., methanol and other oxygenated hydrocarbons. Therefore, the plasma chemistry model indicates that H₂O might not be a suitable H-source for the direct formation of oxygenated hydrocarbons, because of the abundance of O atoms, O₂ molecules and OH radicals in the plasma, trapping the H atoms. We believe that a catalyst will be needed in order to produce significant amounts of oxygenated hydrocarbons in a CO₂/H₂O plasma, and more specifically a catalyst (or catalytic system) that is able to (i) scavenge the O atoms, so that the H atoms can recombine into H₂, before they react with O atoms into OH and H₂O, and (ii) transform the H₂ together with CO into methanol, before CO recombines with OH into CO₂.

Finally, the kinetic analysis also reveals why H₂O₂ is formed in larger amounts upon higher H₂O contents in the mixture, because the OH radicals (as well as the HO₂ radicals) formed from H₂O splitting, will easily recombine into H₂O₂. A summary of the reaction pathways in the CO₂/H₂O mixture is given in Figure 16. A more detailed explanation about the mechanisms can be found in [111]).

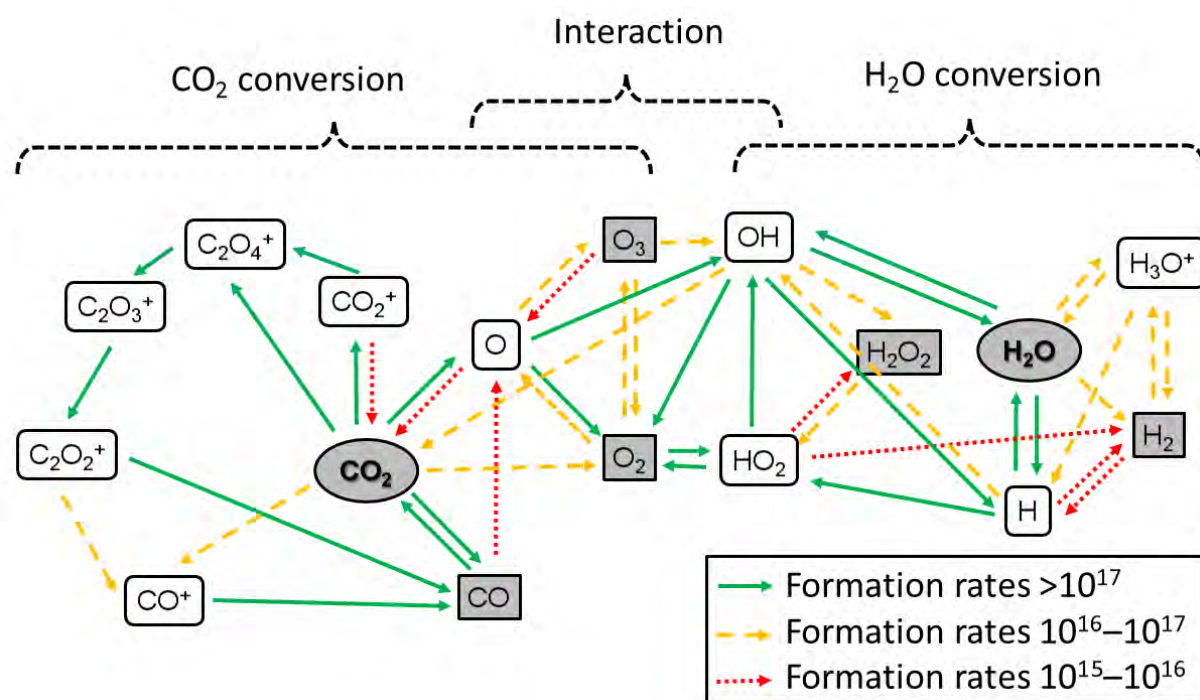


Figure 16: Dominant reaction pathways for the conversion of CO₂ and H₂O and their interactions in a DBD plasma, as obtained from the model in [111]. The full green lines are the formation rates above $10^{17} \text{ cm}^{-3} \text{ s}^{-1}$, the yellow dashed lines indicate formation rates between 10^{16} and $10^{17} \text{ cm}^{-3} \text{ s}^{-1}$, while the red dotted lines are the formation rates between 10^{15} and $10^{16} \text{ cm}^{-3} \text{ s}^{-1}$.

We can conclude that, although a $\text{CO}_2/\text{H}_2\text{O}$ plasma might not be suitable for the direct formation of oxygenated hydrocarbons, it seems to be able to produce H_2/CO ratios in a wide range between 0.0076 and 8.6, and this ratio can be controlled by the H_2O content in the mixture and the SEI value. Furthermore, also significant amounts of H_2O_2 , up the % range, can be formed. The latter can be easily separated by condensation, together with water, and used as disinfectant or for biomedical purposes.

(g) CO_2/N_2 mixture

Real industrial gas flows typically do not contain pure CO_2 , but they are a mixture consisting of other gases and impurities. In most cases, N_2 is the most important component [135]. Therefore, it is of great interest to investigate how the CO_2 conversion and energy efficiency are affected in the presence of N_2 , and moreover, which products (e.g., useful products or harmful NO_x compounds) would be formed in this gas mixture. To answer these questions, modeling can again be very valuable. Therefore, a model was developed for a CO_2/N_2 mixture, and validated by experiments, both for a MW plasma [113] and for a DBD plasma [114], in order to compare both setups in terms of conversion and energy efficiency, as well as in terms of the species formed. This model does not only include the vibrational levels of CO_2 , but also those of N_2 (see Table 1 above), because of the important role of the vibrational kinetics in a MW plasma [121].

Figure 17(a) illustrates the calculated and measured absolute CO_2 conversion as a function of N_2 content, for both a DBD and MW plasma, as obtained from [113,114]. The DBD reactor operates at atmospheric pressure, while the MW plasma is maintained at a pressure of 2660 Pa, which was needed to allow comparison with the experimental data [113]. To enable a fair comparison between the DBD and MW plasma, the results are presented for the same SEI of 2.7 eV/molec. Note, however, that the SEI in J/cm^3 is significantly lower in the MW plasma ($0.27 \text{ J}/\text{cm}^3$) than in the DBD reactor ($11 \text{ J}/\text{cm}^3$), because of the much lower pressure (2660 Pa vs atmospheric pressure), so there are less molecules per volume. Therefore, comparing at the same SEI in eV/molec provides the most “fundamental” comparison, because it tells us exactly how much energy is going to each molecule (on average).

The absolute CO_2 conversion increases with rising N_2 fraction in both types of plasmas, both in the calculations and the experimental data. The exact trends in the MW plasma are somewhat different, indicating that the underlying chemistry might not yet be 100% captured by the model. As the agreement is much better for the DBD reactor, we expect that the discrepancy is related to the vibrational kinetics, which are important in the MW plasma and more or less negligible in the DBD reactor, as explained above. We think that the model could be further improved by adding a more detailed description of the vibrational kinetics, e.g., by including in more detail the symmetric mode levels, so that molecules can exchange vibrational energy with each other, as well as within one molecule. The energy levels close to the dissociation limit then become so close to each other that they form a quasi-continuum, which is currently not taken into account. Furthermore, the rate coefficients of the reactions of the vibrational levels are based on scaling laws, and more accurate scaling laws would probably also improve the accuracy of the model predictions.

Nevertheless, the absolute values are in reasonable agreement. This rising trend indicates that N_2 has a beneficial effect on the CO_2 splitting, in both types of plasmas, but the mechanism appears to be completely different, as is elucidated by the model. In the DBD reactor, the electronically excited metastable $\text{N}_2(\text{A}^3\Sigma_u^+)$ molecules are responsible for the enhanced CO_2 splitting, giving rise to CO , O and ground state N_2 molecules. In the MW plasma, on the other hand, CO_2 is mainly dissociated through the vibrationally excited CO_2 levels. Indeed, these levels are much more populated in the MW plasma than in a DBD, as outlined above, and this is especially true in CO_2/N_2 gas mixtures, because N_2 helps to populate the CO_2 vibrational levels, by VV relaxation processes [113]. As the CO_2 dissociation from vibrationally excited levels is much more efficient than dissociation from the ground state, this also explains the higher CO_2 conversion in the MW plasma than in the DBD reactor, as illustrated in Figure 17(a).

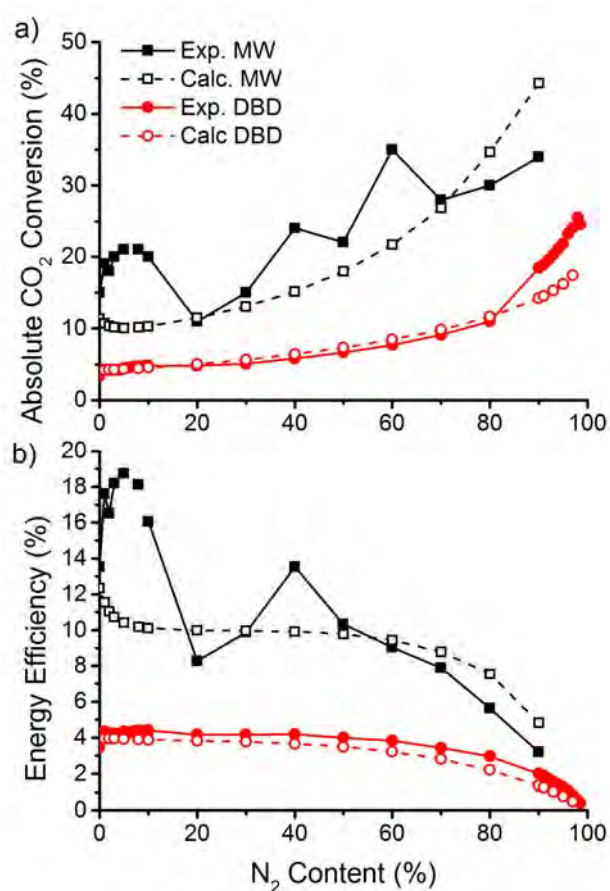


Figure 17: Calculated (dashed lines) and measured (solid lines) absolute CO_2 conversion (a) and energy efficiency (b) as a function of N_2 content in the gas mixture, for a MW plasma at 2660 Pa (black) and a DBD reactor at atmospheric pressure (red), at the same SEI of 2.7 eV/molec, as obtained from the model and experiments described in [113,114].

In spite of the higher absolute CO_2 conversion when adding N_2 to the plasma, the effective or overall CO_2 conversion will drop, because of the lower absolute fraction of CO_2 in the gas mixture. The effect is minor up to about 60% N_2 in the mixture, but more pronounced for higher N_2 fractions. This effective CO_2 conversion determines the overall energy efficiency of the process, which is illustrated as a function of N_2 content, for both the DBD and MW plasma, in Figure 17(b). Because of the somewhat lower effective CO_2 conversion at high N_2 fractions, it is not surprising that the energy efficiency also drops when adding more N_2 to the mixture, as some of the energy is used for ionization, excitation and dissociation of the N_2 molecules. Moreover, both the calculated and measured energy efficiency appear to be a factor 2-3 higher in the MW plasma than in the DBD reactor, for the reason explained above.

Finally, both the modeling and experimental results reveal that several NO_x compounds are produced in the CO_2/N_2 plasma, especially NO , NO_2 , N_2O and N_2O_5 . Figure 18 shows a detailed comparison between their calculated concentrations and the corresponding experimental data for the DBD plasma, at the same conditions as in Figure 17. The experiments were performed with FTIR, but only for NO and NO_2 a calibration curve was available, allowing to express the measured results in absolute concentrations. For N_2O and N_2O_5 , no calibration curves were available, so the data are only shown in arbitrary units (a.u.), as measured absorbance in the FTIR cell.

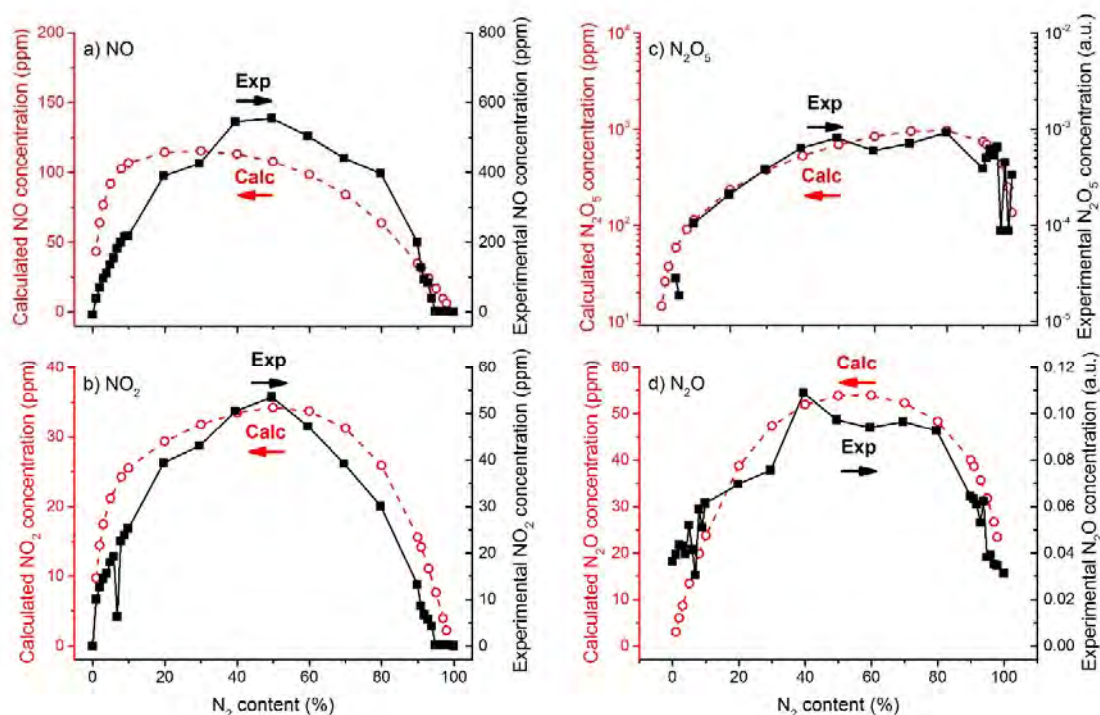


Figure 18: Calculated (red lines, left axis) and measured (black lines, right axis) concentrations of the four main NO_x compounds formed in the CO_2/N_2 DBD plasma, as a function of N_2 content in the mixture, at an SEI of 12 J/cm^3 and a residence time of 0.73 s , as obtained from the model and experiments described in [114]: (a) NO , (b) NO_2 , (c) N_2O_5 , (d) N_2O .

It is clear that both the calculated and measured concentration of each NO_x compound typically reaches its maximum at intermediate N_2 fractions in the mixture (around 50%). Indeed, the NO_x formation is initiated by the reaction of either N atoms or metastable $\text{N}_2(\text{A}^3\Sigma_u^+)$ molecules with O atoms (see below), and these species originate from N_2 and CO_2 , respectively, so it is logical that the maximum NO_x formation is attained when both reactants are present in more or less equal concentrations.

The maximum measured NO and NO_2 concentrations are about 550 ppm and 54 ppm, while the calculated NO and NO_2 concentrations are at maximum 115 and 34 ppm, hence somewhat lower, but still in the same order of magnitude (see Figure 18(a,b)). These values are significantly higher than what is allowed for instance under European emission standards for passenger cars or for industrial emissions (see details in [114]).

The calculated N_2O_5 concentration even reaches values up to 1000 ppm (see Figure 18(c)). It was not possible to obtain absolute concentrations in the experiments, but it is clear that both calculated and measured data show almost the same behavior as a function of N_2 content in the mixture, with a variation over two orders of magnitude over the entire range of N_2 contents. Finally, the maximum calculated N_2O concentration is about 55 ppm (see Figure 18(d)). Although this does not seem to be a very high value, N_2O is a very potent greenhouse gas, with a global warming potential (GWP) 300 times higher than for CO_2 . Based on the absolute CO_2 conversion, plotted in Figure 17(a) above, and the fraction of CO_2 in the mixture, it is clear that effectively about 4 % CO_2 is converted at the conditions under study. Hence, this means that if the N_2O

concentration would exceed 130 ppm, the reduction in GWP by converting CO₂ in the presence of N₂ would effectively be zero. Thus, the production of N₂O seriously limits the greenhouse gas mitigation potential of plasma technology in this case.

In general, although the NO_x concentrations remain in the ppm range, these values are quite significant, and they may cause serious environmental problems. A detailed chemical kinetics analysis, as obtained from the model, can help us to find out how the NO_x formation can be reduced. An overall reaction scheme is illustrated in Figure 19. Initially, N₂ is excited to a metastable state N₂(A³Σ_u⁺), as well as dissociated into N atoms, both upon electron impact. The N₂(A³Σ_u⁺) molecules react with O atoms to create NO, or with O₂ to form N₂O. The N atoms react with both O and O₃ into the formation of NO. NO can be converted into NO₂ upon reaction with O, but the opposite reaction, due to collision with either O or N atoms, occurs as well, making NO₂ the main source of NO production and vice versa.

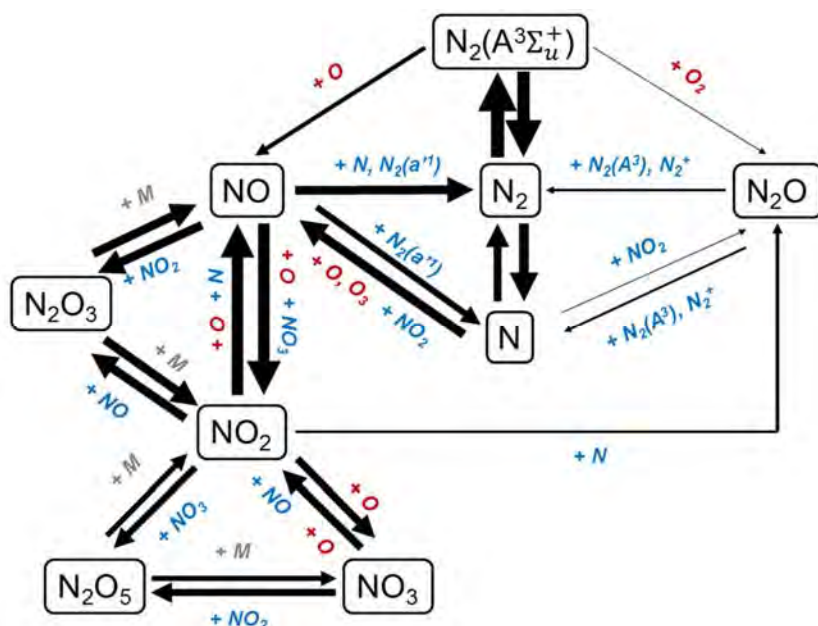


Figure 19: Dominant reaction pathways leading to NO_x formation in a CO₂/N₂ DBD plasma, as obtained from the model in [114]. See details in the text. The thickness of the arrow lines corresponds to the time-integrated reaction rates, indicating the importance of the reactions.

After these initial reactions, the N atoms are trapped in two reaction loops, i.e., between NO, NO₂ and N₂O₃, and between NO₂, NO₃ and N₂O₅. Note that the NO₃ and N₂O₃ concentrations in the plasma are very low, and therefore they were not presented in Figure 18 above. The only way to escape from these loops, is by the reaction of NO₂ to N₂O (which can react back to N₂ and N upon collision with N₂(A³Σ_u⁺) and N₂⁺), or by the reaction of NO with either N atoms or N₂(a¹Σ_u⁻) molecules, forming again N atoms or N₂ molecules (see Figure 19).

Note that the reaction scheme illustrated in Figure 19 applies to a DBD plasma. In a MW plasma, the NO_x formation occurs mainly through the reaction of vibrationally excited N₂ molecules with O atoms, forming N and NO, as explained in [113]. Due to the higher CO₂ (and N₂) conversion in the MW plasma, the formation of NO_x compounds will also be somewhat higher than for the DBD plasma, but the concentrations were still found to be in the ppm range [113]. Note that if concentrations in the % range would be formed, it could be interesting for N-fixation [136], but

the values obtained at the conditions under study are too low to have some economic value and instead they cause an ecological/economic cost.

Thus, if we want to avoid the formation of NO_x compounds, it is clear from the reaction pathways in Figure 19 that the reaction between the reactive N-species (i.e., $\text{N}_2(\text{A}^3\Sigma_u^+)$ and N in a DBD plasma, or vibrationally excited N_2 molecules in a MW plasma) and the O species (O, O_2 or O_3) should be prevented. Reducing the concentrations of reactive N-species in the plasma is not straightforward. Hence, we believe that the only option to avoid NO_x formation, is to remove the O atoms from the plasma, by means of O-scavengers, or separation membranes or a catalytic system, as this would also inhibit the formation of O_2 and O_3 . If the latter could be successful, it would effectively eliminate NO_x formation, and thus the need for either a pre-purification (N_2) or post-purification (denox) step.

(h) CH_4/N_2 mixture

Finally, we present here some results on the effect of N_2 addition on the CH_4 conversion into H_2 in a DBD, both as impurity (up to 50,000 ppm), which is always present in natural gas, and as additive gas (in the range between 1% and 99%), to investigate whether this gas mixture gives rise to the formation of nitrogenated compounds, which could also be of interest for the chemical industry.

Figure 20 illustrates the absolute CH_4 conversion (a), the effective CH_4 conversion (b), and the corresponding absolute and effective H_2 yields (c,d), as a function of N_2 admixture, as obtained from the calculations as well as from experiments. It is clear that the calculations and experiments are in very good agreement.

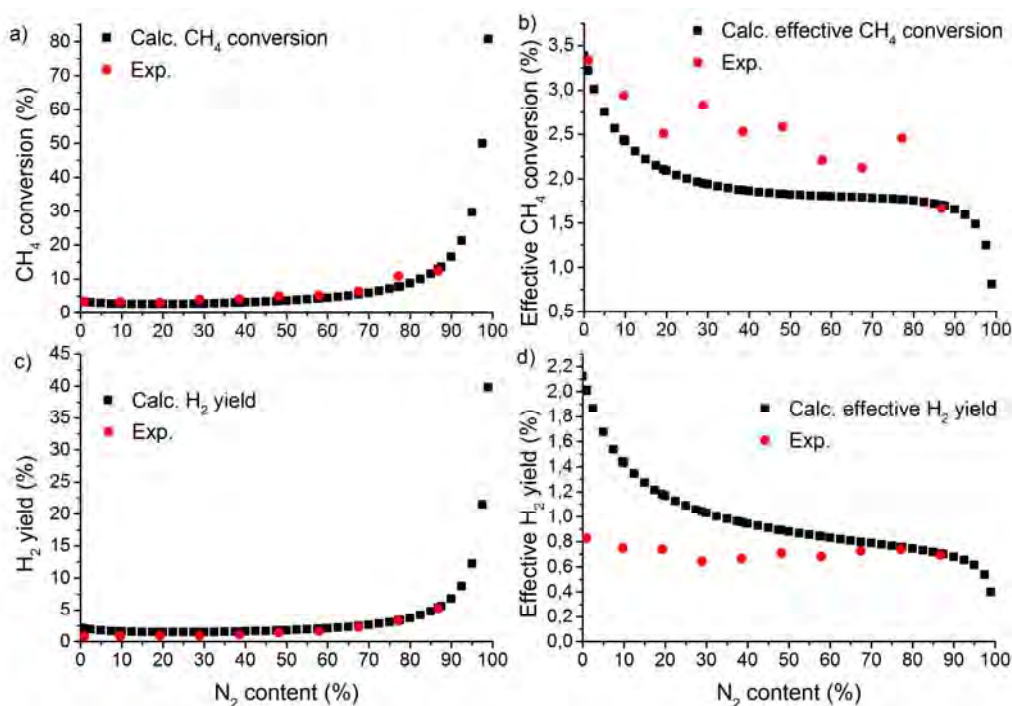


Figure 20: Calculated and measured absolute CH_4 conversion (a), effective CH_4 conversion (b), absolute H_2 yield (c) and effective H_2 yield (d), as a function of N_2 content in the mixture, for an SEI of 6 J/cm^3 and a residence time of 2.2 s , as obtained from the model in [120].

For N_2 contents up to 17.5%, the absolute CH_4 conversion slightly drops from 3.4% to 2.6% (barely visible in figure 20(a), but we refer to [120] for more details). This drop was also observed in the ppm range [120]. However, above 17.5% N_2 content, the absolute CH_4 conversion starts rising nearly exponentially upon increasing N_2 fraction, which is mostly visible above 70%. A kinetic analysis based on the model results indicates that this trend is the result of two competing effects, i.e., the initial drop in CH_4 conversion is due to a lower electron density at higher N_2 content, while the subsequent rise in CH_4 conversion is attributed to the increasing role of N_2 metastable molecules for CH_4 dissociation, as well as the lower reaction rate constants for several three-body recombination reactions of CH_3 radicals back into CH_4 , upon collision with N_2 vs. CH_4 as third body.

The effective CH_4 conversion, which is the product of the absolute CH_4 conversion with the CH_4 content in the mixture, clearly drops upon increasing N_2 content, as is obvious from Figure 20(b). This result is somewhat different from the CO_2/N_2 mixture (see previous section and [113,114]), where the effective CO_2 conversion was more or less constant up to 60% N_2 content, and started decreasing only for higher N_2 contents, because the absolute CO_2 conversion showed a more pronounced increase upon rising N_2 content. Thus, the N_2 molecules (or more specifically, their metastable electronically excited or vibrationally excited levels) are more effective in enhancing the CO_2 conversion than the CH_4 conversion. Overall, the CH_4 conversion is only a few %, reflecting the high stability of CH_4 in a DBD plasma.

The absolute and effective H_2 yield, plotted in Figure 20(c,d) follows the same trend as the CH_4 conversion, with a nearly exponential rise for the absolute yield, but a drop in the effective yield, due to the lower CH_4 content in the mixture upon rising N_2 content. This behavior is quite logical, as CH_4 is the main source of the H atoms. The somewhat lower experimental data are probably attributed to some polymerization at the reactor walls, which was visible in the experimental setup of [120], but not accounted for in the 0D chemical kinetics model. Besides, determining the H_2 yield with a gas chromatography (GC) system is in general quite challenging.

Figure 20 only illustrates the H_2 yields, as this is the major reaction product. Indeed, as is clear from Figure 21, according to the model of [120] the H_2 density is almost one order of magnitude higher than the second most important reaction product (C_2H_6), while the other hydrocarbons have even lower densities, both predicted by the model and detected by GC. Still, the H_2 selectivity is calculated to be only around 40-60%, for all gas mixing ratios investigated, indicating that for every mole of CH_4 converted only 1 mole of H_2 is formed, while the remaining H atoms are consumed for the production of higher hydrocarbons.

Figure 21 also illustrates that the CH_4 density drops upon increasing N_2 content, while the N_2 density rises, which is logical. Furthermore, the H_2 density is more than one order of magnitude lower than the CH_4 density, which could indeed be expected as the CH_4 conversion is only a few % (see Figure 20). Finally, the simulations reveal that some nitrogenated compounds are formed, i.e., HCN and NH_3 , but only at very low densities. Likewise, these products were also not detected in the experiments. This can be explained from the model because the electron energy appears to be too low for efficient ionization of N_2 , which is expected to be the dominant precursor for the formation of these nitrogenated compounds [137].

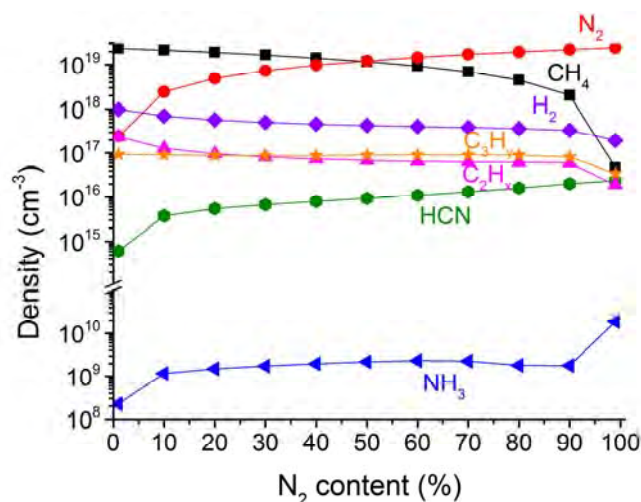


Figure 21: Calculated densities of CH_4 , N_2 , H_2 , higher hydrocarbons, as well as HCN and NH_3 , as a function of N_2 content in the mixture, for an SEI of 6 J/cm^3 and a residence time of 2.2 s , as obtained from the model in [120].

3.2. 2D or 3D fluid modeling

In this section, we will show some fluid modeling results, again mainly obtained within our group, complemented with some data from literature, for the packed bed DBD reactor, MW plasma, and the classical and reverse vortex flow GA reactors, to illustrate their characteristic features, and also to indicate how 2D or 3D fluid models can help to obtain a better insight in the basic characteristics of these plasma reactors. The latter will be useful in the future for improving the reactor design towards a better CO_2 conversion and energy efficiency.

(a) Packed bed DBD reactor

Of the various models developed in literature for a packed bed DBD reactor, the 2D fluid model of Kushner and coworkers [43] is particularly interesting. The packed bed reactor is constructed out of dielectric rods, and the authors studied in detail the mechanism of discharge propagation in humid air. They reported that the discharges in a packed bed reactor can in general be classified in three modalities: positive restrikes, filamentary microdischarges and surface ionization waves. The restrikes are formed after breakdown in regions of high electric field. When they are confined between two dielectrics, they generate filamentary microdischarges that bridge the gap between the dielectrics. Eventually, surface charging near the feet of the microdischarges creates electric field components parallel to the dielectric surface, creating surface ionization waves. The calculations revealed that the production of reactive species primarily takes place near the surfaces, as a result of restrikes and surface ionization waves. In other words, the production of reactants in a packed bed reactor is not a continuous process, but it seems to result from the accumulation of individual, transient events.

The same authors also studied the effect of separation between the dielectric rods and of the rod orientation in the packed bed reactor, and they reported that the type of discharge dominating the production of reactive species depends on the dielectric facilitated electric field enhancement, which is determined by the topography and orientation of the dielectric lattice [43]. While filamentary microdischarges and subcritical discharges and their follow-on negative streamers are stable and occupy

relatively large volumes in the reactor, they might not significantly contribute to the plasma chemical processes, because of their lower electron densities and temperatures. On the other hand, restrikes and surface ionization waves have higher electron densities and temperatures, and thus, in spite of their smaller volume and lifetime, they often produce larger amounts of reactive species. As the packed bed geometry affects the type of discharge that is favored, it will thus also affect the magnitude and reproducibility of reactant production.

Finally, the authors reported that photoionization plays an important role in discharge propagation through the dielectric lattice, because it seeds initial charge in regions of high electric field, which are difficult to access for electrons from the main streamer. This implies that knowledge of the UV spectral distribution is important for studying the propagation of discharges through packed bed reactors [43].

Figure 22 illustrates the calculated time-integrated densities of excited N_2 species, as obtained from the model in [43], together with experimental data, recorded by fast camera imaging of visible light emission in the same type of packed bed reactor with dielectric rods, as studied in the model. In both the simulated and experimental results we can observe the formation of a cathode-seeking filamentary microdischarge (FM) between the rods. In addition, surface ionization waves (SIW) can be seen, due to ions produced in the positive polarity FM, which are accelerated toward the surface of the central rod, positively charging its surface, and thus producing an electric field component parallel to the surface, leading to a SIW. More details about these mechanisms can be found in [43].

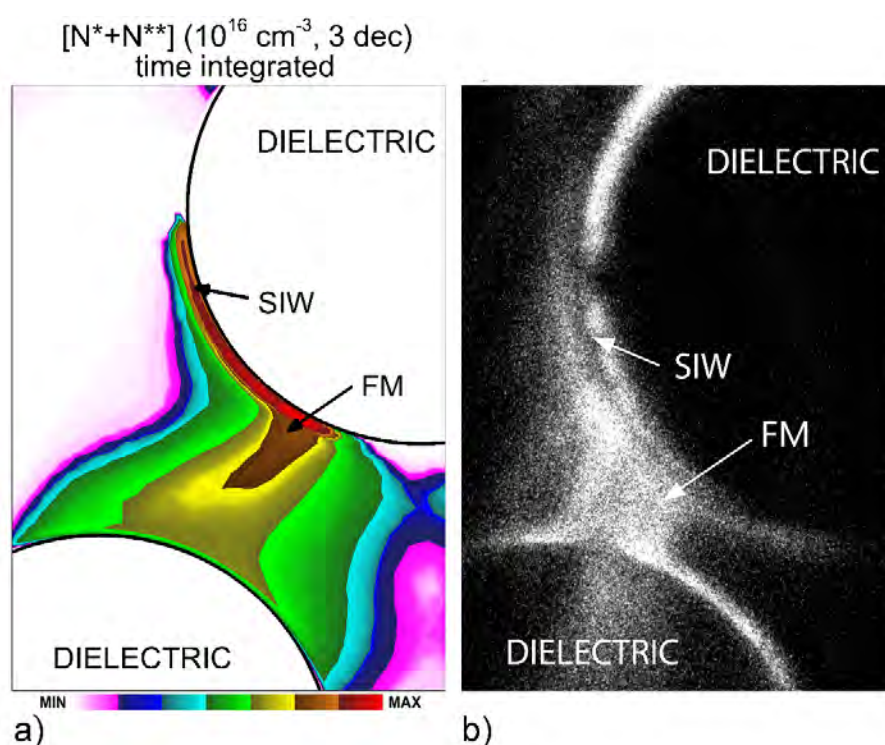


Figure 22: Calculated time-integrated densities of excited N_2 species in a packed bed reactor with dielectric rods, operating in humid air, at an applied voltage of -30 kV and bead separation of 0.7 mm, obtained from 2D fluid simulations by Kushner and co-workers (a), and measured visible light emission, recorded with an ICCD camera at an observation gate width of $0.5 \mu\text{s}$, in the same packed bed reactor as studied in the model (b). Reproduced with permission from [43].

Within our group, we also developed a 2D fluid model for a packed bed DBD reactor, with spherical beads, as explained in section 2.2. Figure 23 illustrates the time-averaged electric field and electron temperature distributions in a 2D representation of a packed bed DBD reactor, for a peak-to-peak voltage of 4 kV and a frequency of 23.5 kHz, both for the “contact point” model (a,b) and the “channel of voids” model (c,d) (cf. Figure 1 above). The “contact point” model clearly illustrates the local electric field enhancement near the contact points, due to polarization of the beads, both inside the material and in the gas gap (see Figure 23(a)). The latter gives rise to more electron heating, which is reflected by the higher electron temperature near the contact points, in Figure 23(b). The same behavior can also be seen in the results of the “channel of voids” model (see Figure 23(c,d)), although it is somewhat less pronounced, because the beads are not in direct contact with each other. The reality will probably be somewhere in between (cf. the description of both 2D models, to mimic the 3D geometry, as presented in section 2.2 above). At this relatively low applied voltage of 4 kV, the plasma is initiated at the contact points, and remains in this region, reflecting the properties of a Townsend discharge. At higher applied voltage, e.g., 7.5 kV (peak-to-peak), the discharge will spread out more into the bulk of the reactor, from one void space to the other, and ultimately covering the whole gas gap, showing the properties of a glow discharge. More details about this behavior can be found in [44].

Validation of these calculation results with experimental data is difficult, because the presence of a packing makes plasma diagnostics not straightforward, e.g., due to visual blocking of optical diagnostics. However, a qualitative comparison is possible with experiments performed by Kim and coworkers, by means of an intensified charge coupled device (ICCD) camera [138,139]. Indeed, these authors also observed that at low applied potential the discharge stays local at the contact points, while at higher potential, it spreads across the surface of the packing material. Similar observations were also made by Tu et al. [140].

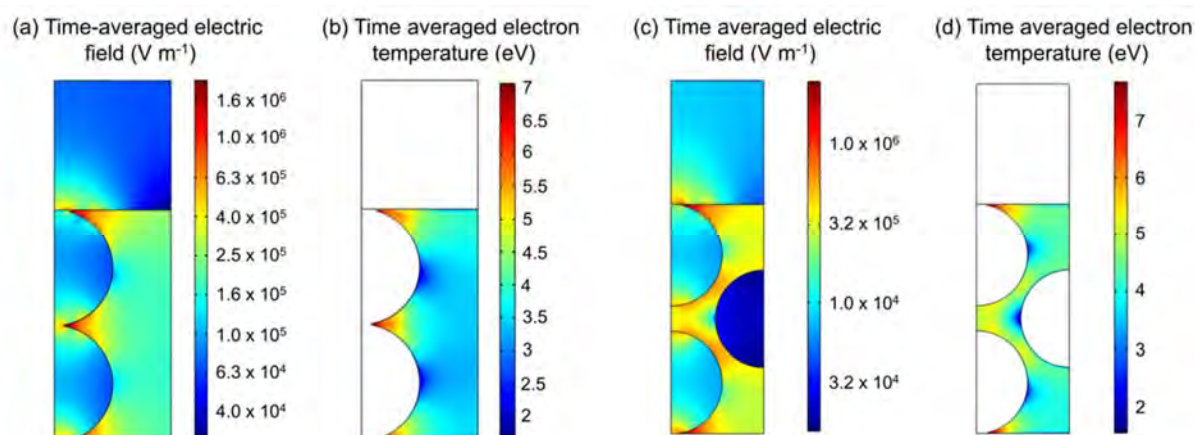


Figure 23: Calculated time-averaged 2D profiles of the electric field and electron temperature in a packed bed DBD reactor, for the two 2D geometries illustrated in Figure 1, i.e., a “contact point” geometry (a,b) and a “channel of voids” geometry (c,d), at a peak-to-peak voltage of 4 kV and a frequency of 23.5 kHz, as obtained from the model in [44].

Although the above models are developed for helium, we expect a similar behavior in a CO₂ plasma. The higher electron temperature will result in more electron impact ionization, excitation and dissociation of the CO₂ molecules, for the same applied power, and this can explain why a packed bed DBD gives a higher CO₂ conversion and energy efficiency than an empty reactor (e.g., [14,18]).

(b) MW plasma reactor

In Figure 24 the calculated electron density, electron temperature, gas temperature and MW electric field distributions are plotted, for the MW surfaguide setup illustrated in Figure 2 above, at a pressure of 700 Pa, a gas flow rate of 125 sccm, a frequency of 2.45 GHz and a power of 100 W.

The electron density (Figure 24(a)) reaches a maximum value of $7 \times 10^{19} \text{ m}^{-3}$ in front of the waveguide (located at $z = 30 \text{ cm}$), and decreases more or less linearly in the axial direction, from the center towards the ends of the plasma. At the same time, it exhibits a wave-like pattern, as a result of resonance due to the metallic grids (indicated with white dashed lines; cf also Figure 2 above). The electron temperature (Figure 24(b)) is fairly constant at about 1.3 eV, in the entire plasma volume, at least within the region confined by the metallic grids. The gas temperature (Figure 24(c)) shows a maximum of 1500 K at the position of the waveguide, i.e., the position of maximum power deposition. Finally, the electric field due to the MW power (Figure 24(d)) shows a pronounced maximum near the walls, indicating the skin effect, and low values in the center of the plasma. Furthermore, the metallic grids clearly prevent any leakage of the electric field outside of the cavity. These results are in reasonable agreement with data from literature, for a similar setup and a similar pressure [141].

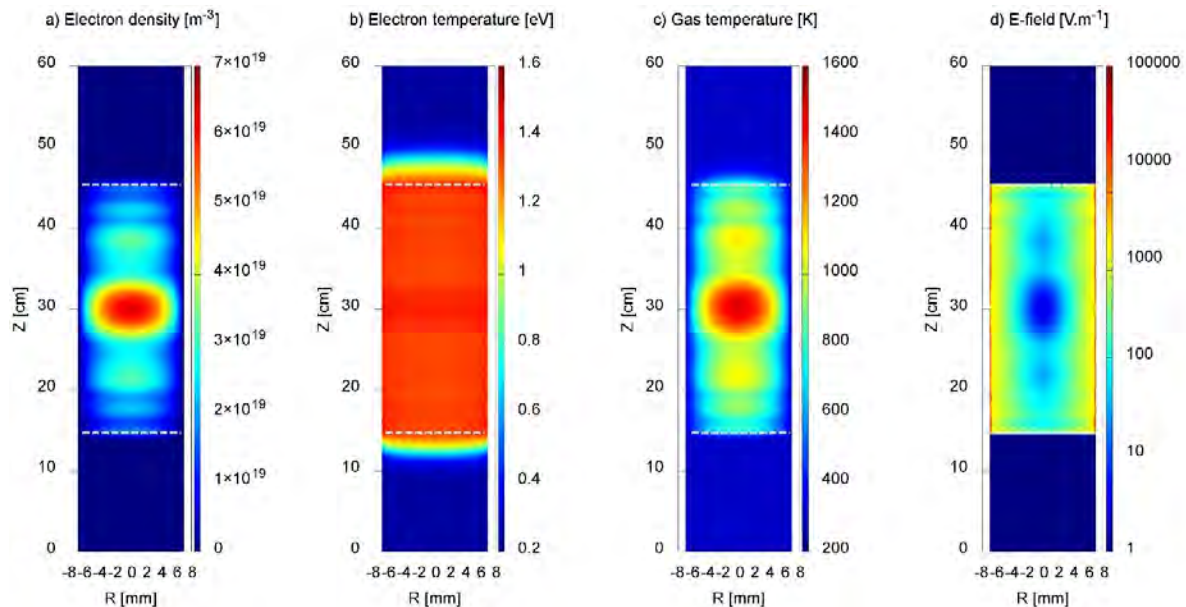


Figure 24: Calculated 2D distributions of electron density (a), electron temperature (b), gas temperature (c) and MW electric field (d), at 700 Pa, a gas flow rate of 125 sccm, a frequency of 2.45 GHz and a power of 100 W, as obtained from the (non-quasi-neutral fluid) model described in [46].

As mentioned in section 2.2(b) above, we aim to extend this model to a CO_2 plasma, so that, besides the above quantities, also information can be obtained about the reactive species densities (including the vibrational levels), the CO_2 conversion and the energy efficiency. If the entire plasma chemistry set would be introduced in the model, as listed in Table 1 above, it would yield excessively long calculation times. Therefore, the chemistry set was recently reduced, from 126 species to 36 or 39 species (depending on pressure, see details in [85]). This reduced set still accounts for all CO_2 vibrational levels, i.e., 21 levels of the asymmetric stretch mode and 4 combined symmetric mode levels (see Table 1 above), because the vibrational kinetics play a key role in energy-efficient CO_2 conversion, as mentioned above. However, to further reduce the chemistry set, a lumped-levels model was developed that allows to lump the 21 vibrational levels of the asymmetric stretch mode into a number of groups [85]. The effectiveness of this

level-lumping strategy was investigated for 1, 2 and 3 groups. Using more groups was found to be redundant, and will be less effective for reducing the calculation time. The models with either 1, 2 or 3 groups were all able to predict the same gas temperature, electron density and electron temperature profiles as in the full model, but like in the GA case (see section 2.2(c) above) only the model with 3 groups can reproduce the shape of the vibrational distribution function (VDF) and thus gives the most reliable prediction of the CO₂ conversion. More details about this level lumping strategy can be found in [85].

As a result of this level lumping, the 21 balance equations for the 21 individual vibrational levels were removed from the model, yielding only 15 (or 18) equations (depending on the pressure; see above) for the remaining plasma species, plus 2 equations for each of the groups (i.e., one equation for the density of the group and one equation for its mean vibrational energy). In this way, a model with n groups needs to solve $15 + 2n$ equations (or $18 + 2n$, depending on pressure) for the chemical kinetics part. This means a reduction in calculation time, and it will open possibilities for describing the CO₂ conversion in a 2D (or even 3D) MW plasma model. This work is currently in progress in our group.

(c) Classical GA plasma

Figure 25 presents the time-evolution of the electron density in a classical GA reactor, as obtained from the model in [59], illustrating the expansion of the gliding arc. Indeed, the arc is dragged by the gas flow, so it bends downstream, and the anode arc root moves upward. To allow the cathode spot to move as well, a so-called field enhancement factor was applied in a limited region, at a point downstream, corresponding to the position of the anode arc root, which initiates a second cathode spot. Thus, the cathode spot is jumping from one point to another, and this results in the so-called “gliding” process of the arc. This procedure was explained in detail in [59].

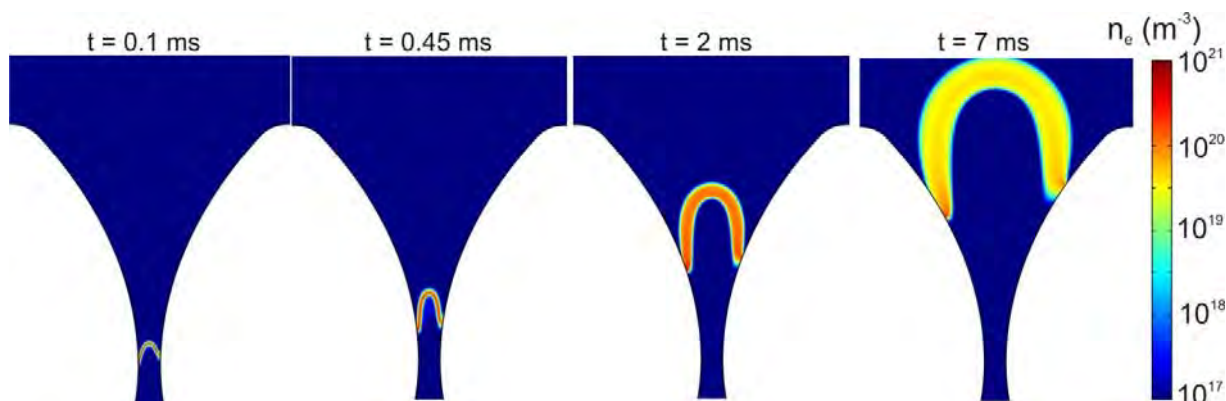


Figure 25: Calculated electron density at different moments in time, as obtained from the model in [59], illustrating the arc evolution during one cycle, from ignition at the shortest interelectrode distance, until extinction.

In spite of its name, the gliding arc can also operate in glow mode. Both discharge modes (i.e., arc and glow) produce a very similar plasma column at a similar discharge current. However, substantial differences are observed near the cathode, due to the different electron emission mechanisms. Indeed, in the glow regime, the cathode root follows the anode root, while in the arc regime, the cathode root remains connected to an electron emission center for a longer period of time, until it jumps to the next position, following the anode root displacement, as explained above. This different way of attachment of the plasma channel to the cathode will result in a longer plasma column in the arc regime than in the glow regime, as was also explained in [60]. The latter can affect the CO₂ conversion in a GA. Indeed, a longer plasma channel means an increased plasma volume, and this will lead to a stronger plasma-gas interaction, possibly leading to more CO₂ conversion. This issue was also briefly discussed in section 3.1(a)

above. The regime that will occur most in practice, will depend on the operating conditions and on the conditioning of the cathode. Note that the discharge operation in the two regimes was also demonstrated experimentally in [142], showing qualitatively the same behavior as explained above.

Another characteristic feature of a GA, observed experimentally, is the so-called back-breakdown phenomenon, or backward-jump motion of the GA, which was studied with a fully coupled gas flow – plasma model [62]. Figure 26 shows the time-evolution of the gas temperature, with (a) and without (b) back-breakdown, as calculated by this model. By comparing both figures, it is clear that the back-breakdown phenomenon causes a drop in the gas temperature, as the heat is now spread over a larger domain and not only concentrated within the initial arc channel. Indeed, before the back-breakdown (0.3 ms), the temperature is the same in both cases, but after the back-breakdown, the gas temperature in the center between both electrodes is about 700 K and 890 K (at 0.4 and 0.5 ms, respectively; see Figure 26(a)), which is obviously lower than in the case without back-breakdown, where values of 900 and 1000 K are obtained at the same moments in time (Figure 26(b)). Furthermore, this figure also illustrates that the back-breakdown causes a delay in the arc velocity with respect to the gas flow velocity (cf. the case with and without back-breakdown). Both effects are of great interest for CO₂ conversion applications, as the lower temperature results in more non-equilibrium conditions, which is beneficial for energy-efficient CO₂ conversion, and the delay in arc velocity allows more gas to pass through the arc, which can lead to more CO₂ conversion (as also briefly discussed in section 3.1(a) above).

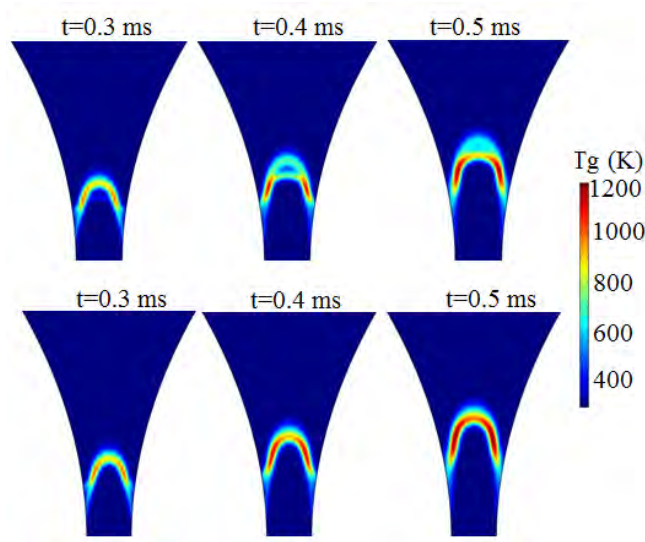


Figure 26: Calculated gas temperature in a GA, at different moments in time, with back-breakdown (upper panels) and without back-breakdown (lower panels), as obtained from the model in [62].

As mentioned in section 2.2 above, within our group we have also developed a 1D cylindrical QN model for a GA, used for CO₂ conversion. Figure 27 shows the number densities of CO₂, CO, O₂, O, and the electrons (a), as well as the electron temperature, the gas temperature and vibrational temperature of the CO₂ asymmetric stretch mode (b), as a function of radial position, as calculated with this model [65]. Note that the radius of the (quasi-cylindrical) arc is assumed to be 2 mm, based on [52,54]. It is clear from Figure 27(a) that CO₂ is the dominant species in most of the arc, except in the very center, where CO has a higher density. This indicates that only within 0.1 mm from the center, a considerable fraction of the CO₂ gas is converted into CO, O and O₂. This can be explained from the electron density profile, as well as the various temperature profiles, depicted in Figure 27(b). Indeed, both the electron density and the various temperatures drop significantly upon rising distance from the center. The electron density is 5

orders of magnitude lower than the gas density, corresponding to a weakly ionized plasma. The electron temperature is almost 3 eV (or 30,000 K) in the center of the arc, but drops to thermal values within 0.5 mm from the center. The vibrational temperature and gas temperature also reach their maximum (i.e., in the order of 2500 K) in the center, and drop significantly upon rising radial distance. The dominant CO₂ conversion mechanisms appear to be dissociation from the CO₂ vibrational levels, either upon electron impact or upon collision with O atoms (see details in [65]). As the vibrational temperature, the O atom density, the electron density and temperature all drop as a function of radial position, it is logical that the CO₂ conversion also drops upon rising radial position, explaining the density profiles shown in Figure 27(a).

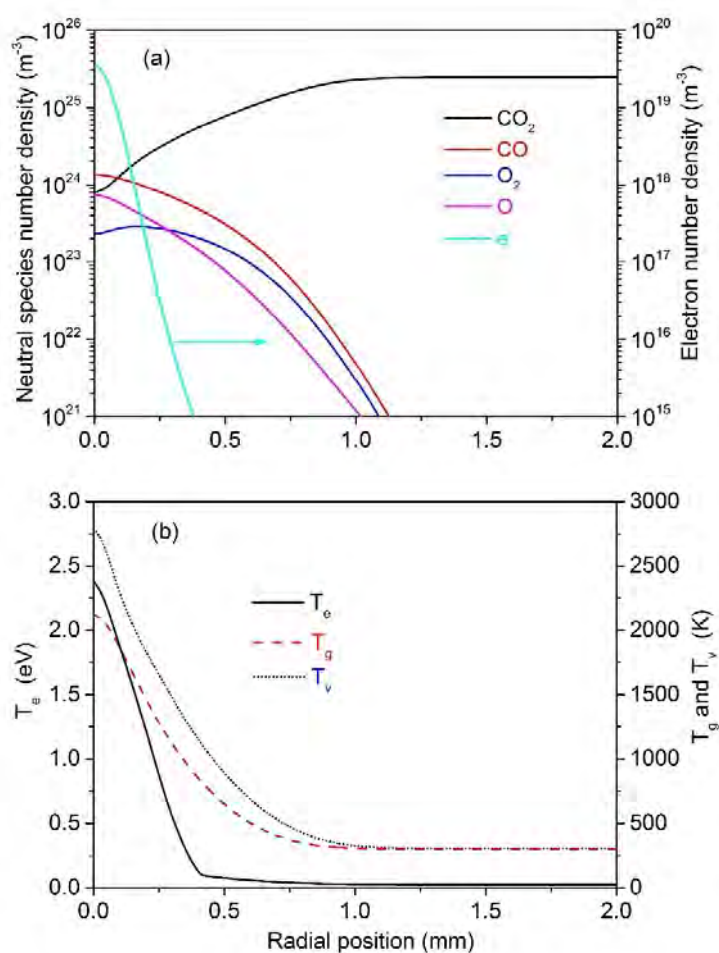


Figure 27: Calculated number densities of CO₂, CO, O₂, O, and electrons (a), and electron, gas and vibrational temperature of the CO₂ asymmetric stretch mode (b), as a function of radial position in the GA as obtained from the model in [65].

The calculated values of electron number density and temperature, gas temperature and vibrational temperature correspond well with experimental data for low current atmospheric pressure gliding arc discharges from literature, as elaborated in [65], although it should be realized that an exact quantitative comparison is not straightforward, due to the different gliding arc setups with different reactor geometries and operating at somewhat different discharge conditions.

(d) Reverse vortex flow GA plasma

In Figure 28 a typical gas flow pattern is plotted, as well as snapshots of the electron density, showing the arc evolution over time, for the reverse vortex flow GA plasma reactor, depicted in Figure 4 above, as obtained from the model in [63].

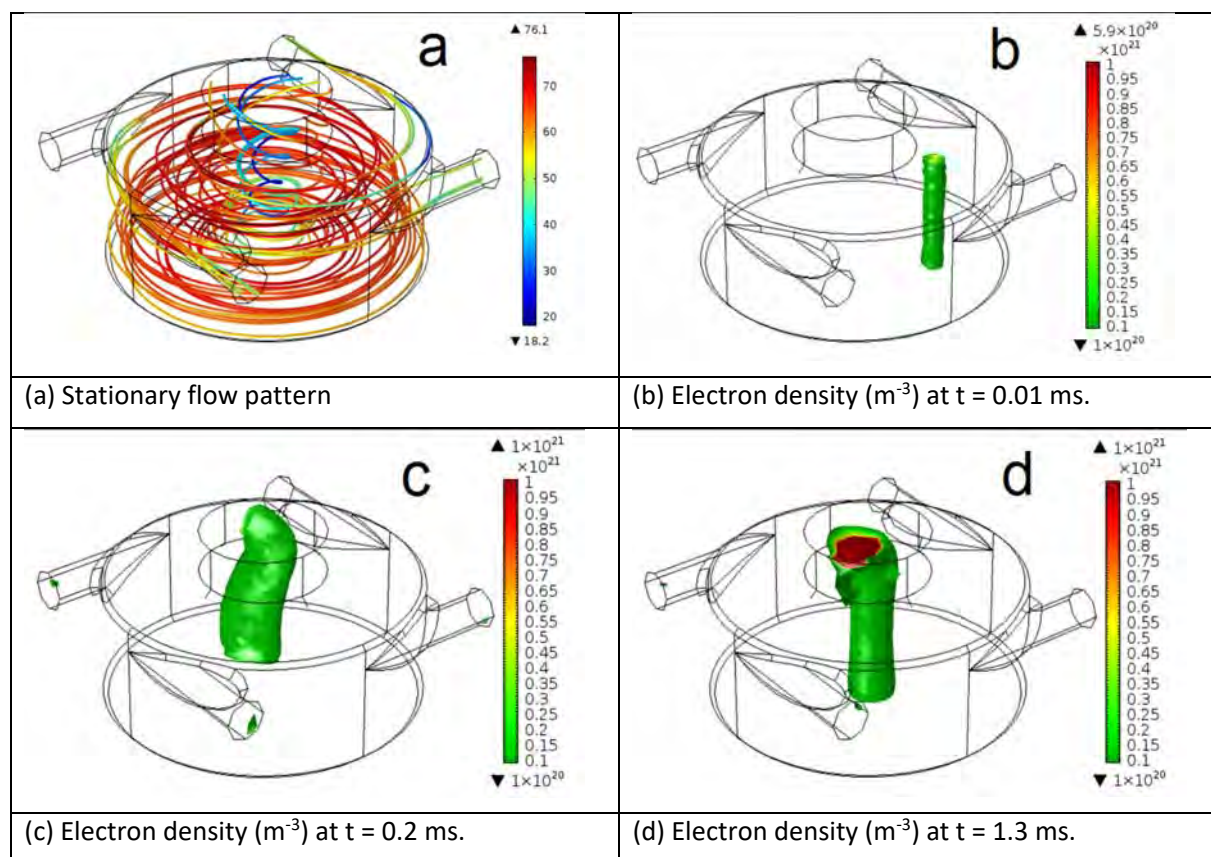


Figure 28: Calculated gas flow pattern (a), and electron density at different moments in time (b,c,d), illustrating the arc evolution over time, for the reverse vortex flow GA plasma reactor of Figure 4 above, as obtained from the model in [63].

After entering the reactor, the gas first flows downwards in an outer vortex, with typical velocities of 70-80 m/s, and then flows upwards in a smaller (inner) vortex, with velocities gradually decreasing to 10 m/s, and finally leaves the reactor through the outlet at the top, as illustrated in Figure 28(a).

From the snapshots of the electron density, it is clear that the arc ignites as a straight plasma column, attached to the outer edge (b) and crawls along the outer edge (c), until it stabilizes at the reactor center, after about 1 ms (d). Thus, the gas, when moving in the inner vortex flow (cf. Figure 28(a)), will largely pass through the arc column. This result is very interesting for the application of CO_2 conversion, as it shows that the design of the RVF GA allows more gas to pass through the arc zone than in a classical (diverging electrodes) GA. From the typical gas velocity (on average 25 m/s) and arc column length (5 mm), we can estimate that the gas residence time in the arc is about 0.2 ms. In this way, the reactor length determines the residence time (given that the plasma arc covers the entire length). Experimental RVF GA reactors usually have greater dimensions. As the arc characteristics are rather uniform over the entire length, this information can be useful for OD modeling, to study in detail the plasma chemistry of CO_2 conversion in a reverse vortex flow GA reactor. This is illustrated in [33].

Conclusion

Plasma-based CO₂ conversion is gaining increasing interest worldwide, but to improve this application, a better insight in the underlying mechanisms is desirable. This insight can be obtained by experiments, but also by modeling. Both plasma chemistry modeling and plasma reactor modeling are important for the applications of CO₂ conversion. This paper shows some examples of both modeling approaches, mainly from our own group, to illustrate what type of information can be obtained from these models, and how this can help to reach a better insight, in order to improve this application.

0D chemical reaction kinetics modeling is very suitable for describing in detail the underlying plasma chemistry of the conversion process. The latter is illustrated in this paper for various gases and gas mixtures of interest, i.e., pure CO₂ splitting, pure CH₄ conversion, CO₂/CH₄, CH₄/O₂, CO₂/H₂ and CO₂/H₂O mixtures, as well as for the effect of N₂ addition to a CO₂ or CH₄ plasma.

It is clear from the models that the underlying chemistry of CO₂ splitting in a DBD plasma is completely different from that in a MW or GA plasma. Indeed, while in a DBD, the CO₂ conversion is attributed to electron impact reactions (mainly electronic excitation followed by dissociation) with the CO₂ ground state molecules, in a MW and GA plasma, vibrational excitation of CO₂ is dominant, and VV relaxation processes gradually populate the higher vibrational levels. This so-called ladder climbing process is the most energy efficient way of CO₂ dissociation, requiring only 5.5 eV per molecule, i.e., exactly the C=O bond energy, while the process of electronic excitation followed by dissociation requires about 7-10 eV per molecule. This “waste of energy” explains the lower energy efficiency of CO₂ splitting in a DBD compared to a MW or GA discharge, as predicted by the models and also reported experimentally (see introduction).

Also for the other gas mixtures, the models reveal that in a DBD plasma the reaction pathways responsible for CO₂ or CH₄ conversion are all initiated by electron impact reactions, and more specifically, mainly by electron impact dissociation, creating radicals that can react further into value-added compounds, such as syngas (CO/H₂), but also higher hydrocarbons and oxygenates. However, as many different radicals and chemical compounds are formed in the plasma, the selective production of targeted compounds is not possible. For this purpose, a catalyst must be inserted in the plasma. Our models show that CO₂/CH₄ and CH₄/O₂ mixtures exhibit totally different chemical reaction pathways, yielding different product distributions. Furthermore, a CO₂/H₂ mixture does not produce many higher hydrocarbons and oxygenates, in contrast to the CO₂/CH₄ and CH₄/O₂ mixtures, and moreover the CO₂ conversion is very limited. This is both attributed to the lack of CH₂ (and CH₃) radical formation in the CO₂/H₂ mixture, as the CH₂ radicals are the main collision parts of CO₂ in the CO₂/CH₄ mixture.

Likewise, the model for the CO₂/H₂O mixture shows that adding H₂O to a CO₂ DBD plasma results in a drop of the CO₂ conversion. Moreover, the H₂O conversion itself is also limited, and virtually no oxygenated hydrocarbons are formed. All these trends could be explained from the chemical reaction pathways. The insight obtained in this way might be useful to provide possible solutions. For instance, our kinetic analysis reveals that no oxygenated hydrocarbons are formed upon H₂O addition to a CO₂ plasma, because the H atoms react with O atoms into OH radicals, and subsequently into H₂O, instead of forming CH and CHO fragments, which are needed to create e.g., methanol and other oxygenated hydrocarbons. To overcome this problem, we believe that a catalyst will be needed, which is able to (i) scavenge the O atoms, so that the H atoms can recombine into H₂, before they react with O atoms into OH and H₂O, and (ii) transform the H₂ together with CO into methanol, before CO recombines with OH into CO₂. On the other hand, the CO₂/H₂O plasma seems to be able to produce H₂/CO ratios in a very wide range, and this ratio can be controlled by the H₂O content in the mixture and the SEI value. This is very useful for Fischer-Tropsch synthesis for the production of liquid fuels, and also for methanol synthesis. Thus, even if methanol

formation seems not feasible in a direct one-step plasma process without catalyst, it might be possible in a two-step process. Furthermore, our model predicts that also significant amounts of H_2O_2 can be formed, up to the % range, which is also a useful compound, e.g., for disinfection or biomedical purposes.

Another example of 0D chemical kinetics modeling is given for a CO_2/N_2 plasma. This is of interest because N_2 is typically a very important component in real industrial gas flows. A comparison is made between DBD and MW plasma conditions, and it is shown that the CO_2 conversion and energy efficiency are clearly higher in the MW plasma, which is again attributed to the vibrational kinetics. In contrast to the $\text{CO}_2/\text{H}_2\text{O}$ plasma, where the CO_2 conversion drops upon H_2O addition, both the calculations and experiments in the CO_2/N_2 plasma demonstrate that N_2 addition enhances the (absolute) CO_2 conversion, both in the DBD and MW plasma. The underlying mechanism is, however, different for both types of plasmas, i.e., it is attributed to the N_2 metastable molecules in the DBD plasma, while in the MW plasma it is due to the N_2 vibrational levels which populate the CO_2 vibrational levels. The CO_2/N_2 mixture, however, also produces NO_x compounds in ppm concentrations, which can give several environmental problems. Again, the model can be used to explain their formation, and this is useful to provide possible solutions on how this NO_x formation can be avoided.

Finally, the last example is given for a CH_4/N_2 mixture, as CH_4 reforming by plasma is also very relevant, and N_2 is always present in natural gas. Furthermore, it is useful to know whether nitrogenated compounds (e.g., HCN or NH_3) could be formed, which would also be of interest for valorization purposes. However, the model reveals that almost no nitrogenated compounds are formed, and this could be explained because of the limited electron impact ionization of N_2 , which was reported in literature to be mainly responsible for the formation of these compounds.

Although 0D models can give useful information on the detailed plasma chemistry, and thus the reaction pathways leading to certain products, they cannot really account for details in the plasma reactor configuration. In order to be able to predict how modifications to the reactor design might lead to improved CO_2 conversion, 2D or 3D fluid models of specific reactor designs are needed. However, developing such fluid models for a detailed plasma chemistry leads to excessive calculation times. Therefore, these models are up to now mainly developed for argon or helium, which are characterized by a more simple chemistry. We have shown here examples of typical calculation results, obtained for the three types of plasma reactors most commonly used for CO_2 conversion, i.e., a packed bed DBD reactor, a MW plasma, and both a classical and reverse vortex flow GA plasma reactor.

In future work, it would be necessary to implement the more complex CO_2 chemistry (either pure or mixed with other gases) in such fluid models, to obtain the complete picture of CO_2 conversion in these plasma reactors. Furthermore, at that stage, it will be necessary to compare the calculation results with experimental data. The most obvious results to be compared are the electrical characteristics, as well as the CO_2 conversion, product yields and energy efficiency, like is done already for the 0D chemical kinetics models, as this information can more easily be obtained in the experiments. Detailed comparison of other calculation results, like spatially resolved plasma species densities, electron temperature, gas temperature, gas flow behavior, and information about the vibrational kinetics, is more difficult to realize at this stage, because the 2D models are still based on some approximations, which make comparison less straightforward, and because of a general lack of experimental data in literature for these plasma reactors. The latter also stresses the added value of modeling. However, we sincerely hope that more experimental data for these plasma reactor types will become available in the near future, to better validate the models.

As mentioned above, implementing more complex plasma chemistries in 2D or 3D models is quite challenging in terms of calculation time. To overcome this problem, reduced chemistry sets must be developed for CO_2 (and its gas mixtures), either without vibrational kinetics, applicable to a DBD reactor

[16], as well as with detailed vibrational kinetics, which is crucial for describing a MW or GA plasma reactor [85]. Furthermore, the level-lumping strategy that was developed in [85] enables to group the vibrational levels of the asymmetric stretch mode of CO₂ into a number of groups, to further reduce the calculation time, as demonstrated in [64,85]. This method opens possibilities for the implementation of more complicated reaction chemistries in 2D (and hopefully in the future in 3D) plasma reactor models, which is of course the ultimate goal of the models to be developed for this application. In general, we believe indeed that a combination of 0D chemical kinetics models (to obtain detailed insight in the entire plasma chemistry, and to develop reduced chemistry sets, identifying the main species and chemical reactions) and 2D/3D fluid models (for a detailed insight in the effect of the reactor design) is the most promising approach to make further progress in this field.

As the modeling results presented here provide an overview of the plasma chemistry for various gas mixtures of interest, and in the three major types of plasma reactors for this application, we can use them to gain further insight in what would be the “ultimate” reactor and reaction conditions to maximize the conversion and energy efficiency, and whether plasma technology is competitive with other emerging conversion technologies, and has the potential to become industrially relevant.

According to the models, the energy efficiency of CO₂ conversion will always be too limited in a DBD. This is attributed to the strong reduced electric field values (200 Td and above), giving rise to relatively high electron energies (several eV), and thereby inducing electron impact electronic excitation, ionization and dissociation of the CO₂ ground state molecules, which are energy inefficient processes. Indeed, they require more energy than strictly needed for the C=O bond breaking, compared to the vibrational pathway, which only requires the strict minimum of 5.5 eV. The conversion can be improved in packed bed DBD reactors, due to the enhanced electric fields at the contact points, causing higher electron energies, as demonstrated by the 2D modeling results presented in this paper, yielding more electron impact processes for the same applied power. However, these processes are obviously still electronic excitation, ionization and dissociation, because for vibrational excitation lower electron energies are needed. Thus we believe that DBD reactors will never yield a sufficiently high energy efficiency for industrial exploitation of pure CO₂ splitting, unless drastically different conditions could be reached, which can tune the reduced electric field down to lower values, suitable for electron impact vibrational excitation, e.g., by novel types of power supplies. It is clear, indeed, that the vibrational pathway for CO₂ dissociation should be targeted to really improve the energy efficiency of this process. On the other hand, packed bed DBD reactors might still be of interest in case of CO₂ mixtures with a H-source, such as CH₄, H₂O H₂, as they easily allow the implementation of a catalyst. If a suitable catalyst can be found to selectively produce chemical compounds with high added value, this might compensate for the limited energy efficiency of the packed bed DBD reactor, because plasma catalysis could then allow the direct production of these value-added compounds, instead of a two-step process through syngas production followed by the Fischer-Tropsch synthesis. However, still a lot of basic research will be needed in the search for suitable catalysts, as the latter might be different from classical thermal catalysts, because of the completely different conditions of plasma catalysis.

On the other hand, the models reveal that a MW and GA plasma are more promising for energy efficient CO₂ conversion, because they are characterized by lower reduced electric field values (order of 50-100 Td), producing electron energies of around 1 eV, which is most suitable for efficient vibrational excitation. However, currently, most MW and GA plasmas do not yet operate at the most suitable conditions to maximize the vibrational pathway, as the conversion process is often too much dictated by thermal processes, as a result of the high gas temperature.

The model calculations clearly demonstrate the need to exploit the non-equilibrium, non-thermal character of a MW plasma, where the higher vibrational levels of CO₂ are overpopulated, as this is crucial

for energy efficient CO₂ conversion. This can be realized when operating at reduced pressure and sufficiently high power densities, while keeping the gas temperature as low as possible, as demonstrated in this paper. On the other hand, for industrial applications, it would be beneficial to work at atmospheric pressure, to avoid the extra cost of pumping, which also contributes to the overall energy cost of the process. We believe there are several possible options to reach these non-equilibrium conditions, while still operating at atmospheric pressure of the CO₂ gas entering the reactor. One option is to work with a supersonic gas flow, as already demonstrated by Asisov et al. in 1983, reaching energy efficiencies of 90% [19], because such a setup can combine a reduced pressure in the plasma region, and a low temperature, with high power density. Another possibility is to apply a reverse vortex gas flow, as currently explored in DIFFER [23], because this leads to gas cooling, as well as stabilization of the plasma at atmospheric pressure. A third option could be to apply pulsed power, which will also allow to reach high power densities, with reduced gas heating. We plan to investigate these options in our future modeling work.

Also in a GA plasma, the models predict that the CO₂ conversion is still too much dictated by thermal processes, due to the relatively high temperature inside the arc region, thus limiting the energy efficiency reached up to now. However, we believe that in a GA plasma there is also clear room for improvement. Indeed, the calculations demonstrate that a significant overpopulation of the higher vibrational levels in the VDF can be realized by decreasing the temperature or by increasing the power density, just like in a MW plasma. The first option can probably be targeted by using a high-frequency discharge, so that the arc has not enough time to heat up. The second option might be realized by using a micro-scale gliding arc reactor, as demonstrated in literature [143], although this will limit the throughput, unless using several reactors in parallel.

Another limitation of a GA, at least in the classical (diverging electrodes) configuration, is the limited gas fraction that passes through the arc. Indeed, the model calculations reveal that inside the arc, the CO₂ splitting into CO and O₂ can reach up to 100%, but the overall CO₂ conversion is limited by the fraction of gas passing through the arc, which is in the order of 10-20 % [144,145]. In addition, as a result of this high conversion, the backward (recombination) reactions become equally important as the forward (dissociation) reactions, thereby limiting the overall conversion. This was convincingly demonstrated in [64], by removing the recombination reaction from the model (see also Figure 9 in this paper). We believe that the backward reactions could be reduced if some chemical scavengers could be added, such as CH₄, which produce H atoms that quickly react with the O atoms, before the latter can recombine with the CO molecules into CO₂. A similar principle was also illustrated both by modeling and experiments in [146] for a DBD to chemically trap the O atoms into H₂O instead of O₂, and thus allowing an easier separation of the products formed. Furthermore, working at lower gas temperature will also reduce the backward reactions, because the O atoms will more efficiently be used for other reactions (e.g. O₃ formation).

Finally, another way to reduce the backward reactions is to make sure that the CO molecules leave the arc discharge zone once they are formed. This could be realized when there is a difference in velocity between the gas flow and the arc movement. In addition, the latter would result in more CO₂ gas that can pass through the arc, thereby also reducing the limited gas fraction that can be treated, which is, in our opinion, the most crucial limitation of (classical) GA discharges. A difference in gas flow velocity vs arc gliding velocity may result from the phenomenon of back-breakdown, which indeed causes a lower gliding arc velocity, as demonstrated by the 2D fluid modeling results presented in this paper, as well as in literature [147-149]. Experimentally, some operating parameters can be adjusted to control the occurrence of the back-breakdown process, such as the gas flow rate, the electrical current and the

reactor/electrode geometry. In addition, the back-breakdown phenomenon will reduce the gas temperature, as illustrated by the model calculations presented in this paper, because the heat will be spread out over a larger region, so this will also be beneficial for exploiting the non-equilibrium conditions of the GA. Finally, applying a different design of the GA reactor, such as in a reverse vortex flow GA, also allows more gas to pass through the arc. Indeed, the 3D model calculations presented in this paper demonstrate that in this setup the gas first flows in a vortex close to the reactor walls to one end of the reactor, followed by an inner vortex in the reverse direction, and that the arc is stabilized in the middle of the reactor, so that this inner vortex passes through the arc, thereby allowing a larger gas fraction to be converted in the arc zone. These model calculations predict that this fraction is around 40 % for the RVF GA reactor developed in [25,27], but this can probably be further improved by modifications to the reactor setup.

In conclusion, the model calculations reveal that there is still room for improvement of the energy efficiency in a MW and GA plasma, by further exploiting the non-equilibrium conditions, and by enhancing the gas fraction that passes through the arc in case of the GA reactor. The most important general message from the models is that, in order to optimize the energy efficiency of CO₂ conversion in any kind of plasma, the vibrational pathway should be maximized, i.e., electron impact vibrational excitation to the lower levels, followed by VV relaxation, gradually populating the higher levels, which can then dissociate upon collision with heavy particles. To reach this, the VDF must be strongly non-thermal, with a pronounced overpopulation of the higher vibrational levels.

We believe that if these non-equilibrium conditions can be further exploited, plasma technology will be competitive with other emerging CO₂ conversion technologies, such as electrocatalytic, photocatalytic and solar thermochemical conversion. All these emerging technologies directly or indirectly use sunlight for the production of fuels. Therefore, the key performance indicator to compare these different technologies is the solar-to-fuel energy conversion efficiency. Photocatalytic and solar thermochemical conversion technologies directly use sunlight. The solar-to-fuel efficiency of photocatalytic conversion is currently less than 2% [150], but a lot of research is performed to improve this number. Nevertheless, the theoretical maximum solar-to-fuel efficiency will be limited to 17 %, due to the band gap energy of the photocatalyst [151]. For solar thermochemical conversion, theoretical solar-to-fuel efficiencies exceeding 30 % are reported, but values above 10 % are still pending experimental demonstration with robust and scalable solar reactors [150,152,153]. It is stated that a value of 20 % is required for solar fuels to become cost competitive [154]. Other novel conversion technologies indirectly use sunlight, the most widespread one being water electrolysis. When using photovoltaic cells, which currently have an efficiency of 25 %, solar-to-fuel efficiencies of 7-10% are reported for water electrolysis [150].

As mentioned in the Introduction, plasma technology also has potential for the temporary storage of excess renewable energy into fuels, during peak production of e.g., solar panels. Hence, assuming that the electricity needed for our plasma process is produced by solar panels, with an efficiency of 25 %, an energy efficiency of 50 % for CO₂ conversion in the plasma, as was predicted by the models under suitable conditions, and which was also experimentally already demonstrated, would yield a solar-to-fuel efficiency of 12.5 %. This value is already better than several other emerging technologies, and close to being cost competitive. Furthermore, we are convinced from the model calculations that there is still room for improvement in the energy efficiency, certainly for a MW and GA, as outlined above. Finally, the overall energy efficiency can be further improved when the efficiency of solar panels will become higher. Furthermore, besides relying on solar-based renewable energy, plasma technology can also take advantage of other sources of renewable electricity. Note that the latter option is obviously not possible

for photochemical and solar thermochemical technologies, which directly use sunlight, pointing towards the higher flexibility of plasma technology.

Acknowledgments

We would like to thank T. Silva, N. Britoun, Th. Godfroid and R. Snyders (Université de Mons and Materia Nova Research Center), A. Ozkan, Th. Dufour and F. Reniers (Université Libre de Bruxelles), K. Van Wesenbeeck and S. Lenaerts (University of Antwerp) for providing some experimental data to validate our models. Furthermore, we acknowledge financial support from the IAP/7 (Inter-university Attraction Pole) program ‘PSI-Physical Chemistry of Plasma-Surface Interactions’ by the Belgian Federal Office for Science Policy (BELSPO), the Francqui Research Foundation, the European Union’s Seventh Framework Programme for research, technological development and demonstration under grant agreement no. 606889, the European Marie Skłodowska-Curie Individual Fellowship project “GlidArc” within Horizon2020, the Methusalem financing of the University of Antwerp, the Fund for Scientific Research Flanders (FWO; Grant no. G.0383.16N and 11U5316N) and the Institute for the Promotion of Innovation by Science and Technology in Flanders (IWT Flanders). The calculations were carried out using the Turing HPC infrastructure at the CalcUA core facility of the Universiteit Antwerpen (UAntwerpen), a division of the Flemish Supercomputer Center VSC, funded by the Hercules Foundation, the Flemish Government (department EWI) and the UAntwerpen.

References

- [1] McDonough W and Braungart M, 2002, *Cradle to Cradle: Remaking the Way We Make Things*, North Point Press
- [2] Centi G, Quadrelli E A and Perathoner S 2013 *Energy Environ. Sci.* **6**, 1711
- [3] Aresta M, Dibenedetto A and Angelini A 2014 *Chem. Rev.* **114** 1709
- [4] Styring P, Quadrelli E A and Armstrong K, 2015, *Carbon Dioxide Utilization: Closing the Carbon Cycle*, Elsevier, Amsterdam
- [5] Paulussen S, Verheyde B, Tu X, De Bie C, Martens T, Petrovic D, Bogaerts A and Sels B 2010 *Plasma Sources Sci. Technol.* **19** 034015
- [6] Pinhao N R, Janeco A and Branco J B 2011 *Plasma Chem Plasma Proc.* **31** 427
- [7] Eliasson B, Kogelschatz U, Xue B and Zhou L-M 1998 *Ind. Eng. Chem. Res.* **37** 3350
- [8] Wang Q, Cheng Y and Jin Y 2009 *Catal. Today* **148** 275
- [9] Zhang A-J, Zhu A-M, Guo J, Xu Y and Shi C 2010 *Chem Eng. J.* **156** 601
- [10] Tu X, Gallon H J, Twigg M V, Gorry P A and Whitehead J C 2011 *J. Phys. D: Appl. Phys.* **44** 274007
- [11] Nozaki T and Okazaki K 2013 *Catal. Today* **211** 29
- [12] Gómez-Ramírez A, Rico V J, Cotrino J, González-Elipe A R and Lambert R M 2014 *ACS Catalysis* **4** 402
- [13] Scapinello M, Martini L M and Tosi P 2014 *Plasma Proc. Polym.* **11** 624
- [14] Mei D, Zhu X, He Y, Yan J D and Tu X 2015 *Plasma Sources Sci. Technol.* **24** 015011
- [15] Ozkan A, Dufour T, Arnoult G, De Keyser P, Bogaerts A and Reniers F 2015 *J. CO₂ Util.* **9** 74
- [16] Aerts R, Somers W and Bogaerts A 2015 *ChemSusChem.* **8** 702
- [17] Ramakers M, Michielsen I, Aerts R, Meynen V and Bogaerts A 2015 *Plasma Process. Polym.* **12** 755
- [18] Van Laer K and Bogaerts A 2015 *Energy Technol.* **3** 1038
- [19] Asisov R I, Givotov V K, Krasheninnikov E G, Potapkin B V, Rusanov V D and Fridman A 1983 *Sov. Phys., Doklady* **271** 94
- [20] Spencer L F, Gallimore A D 2013 *Plasma Sources Sci. Technol.* **22** 015019
- [21] Silva T, Britoun N, Godfroid T and Snyders R 2014 *Plasma Sources Sci. Technol.* **23** 025009

- [22] Goede A P H, Bongers W A, Graswinckel M F, van de Sanden M C M, Leins M, Kopecki J, Schulz A and Walker M 2013 *EPJ Web of Conferences*, 3rd Eur. Energy Conference
- [23] Bongers W, Bouwmeester H, Wolf B, Peeters F, Welzel S, van den Bekerom D, den Harder N, Goede A, Graswinckel M, Groen P W, Kopecki J, Leins M, van Rooij G, Schulz A, Walker M and van de Sanden R 2017 *Plasma Process. Polym.*, DOI: 10.1002/ppap.201600126
- [24] van Rooij G J, van den Bekerom D C M, den Harder N, Minea T, Berden G, Bongers W A, Engeln R, Graswinckel M F, Zoethout E and van de Sanden M C M 2015 *Faraday Discussions* **183** 233
- [25] Kalra C S, Cho Y I, Gutsol A, Fridman A and Rufael T S 2005 *Rev. Sci. Instrum.* **76** 025110
- [26] Indarto A, Yang D R, Choi J-W, Lee H and Song H K 2007 *J. Hazard. Mater.* **146** 309
- [27] Nunnally T, Gutsol K, Rabinovich A, Fridman A, Gutsol A and Kemoun A 2011 *J. Phys. D: Appl. Phys.* **44** 274009
- [28] Lee H and Sekiguchi H 2011 *J. Phys D: Appl. Phys.* **44** 274008
- [29] Tu X and Whitehead J C 2014 *Int. J. Hydrogen Energy* **39** 9658
- [30] Liu J L, Park H W, Chung W J, Park D W 2016 *Chem. Eng. J.* **285** 234
- [31] Liu J L, Park H W, Chung W J and Park D W 2016 *Plasma Chem. Plasma Process.* **36** 437
- [32] Li K, Liu J L, Li X S, Zhu X and Zhu A M 2016 *Chem. Eng. J.* **288** 671
- [33] Ramakers M, Trenchev G, Heijkers S, Wang W and Bogaerts A, *Energy Environm. Sci.* (submitted).
- [34] Scapinello M, Martini L M, Dilecce G and Tosi P 2016 *J. Phys. D: Appl. Phys.* **49** 075602
- [35] Shapoval V, Marotta E, Ceretta C, Konjevic N, Ivkovic M, Schiorlin M and Paradisi C 2014 *Plasma Process Polym.* **11** 787
- [36] Zhu B, Li X S, Shi C, Liu J L, Zhao T L and Zhu A M 2012 *Int. J. Hydrogen Energy* **37** 4945
- [37] Zhu B, Li X S, Liu J L, Zhu X and Zhu A M 2015 *Chem. Eng. J.* **264** 445
- [38] Chang J S, Kostov K G, Urashima K, Yamamoto T, Okayasu Y, Kato T, Iwaizumi T and Yoshimura K 2000 *IEEE Trans. Ind. Appl.* **36** 1251
- [39] Takaki K, Chang J-S and Kostov K G 2004 *IEEE Trans. Dielectrics and Electrical Insulation* **11** 481
- [40] Zhang Y, Wang H-Y, Jiang W and Bogaerts A 2015 *New J. Phys.* **17** 083056
- [41] Kang W S, Park J M, Kim Y and Hong S H 2003 *IEEE Trans. Plasma Sci.* **31** 504
- [42] Russ H, Neiger M and Lang J E 1999 *IEEE Trans. Plasma Sci.* **27** 38
- [43] Kruszelnicki J, Engeling K W, Foster J E, Xiong Z and Kushner M J 2017 *J. Phys. D: Appl. Phys.* **50** 025203
- [44] Van Laer K and Bogaerts A 2016 *Plasma Sources Sci. Technol.* **25** 015002
- [45] Van Laer K and Bogaerts A 2017 *Plasma Process. Polym.* **14**, DOI 10.1002/ppap.201600129
- [46] Georgieva V, Berthelot A, Silva T, Kolev St, Graef W, Britun N, Chen G, van der Mullen J, Godfroid T, Mihailova D, van Dijk J, Snyders R, Bogaerts A and Delplancke-Ogletree M-P 2017 *Plasma Proc. Polymers* (in press)
- [47] Janssen G M 2000 PhD Thesis, Eindhoven University of Technology, the Netherlands
- [48] Jimenez-Diaz M, Carbone E A D, van Dijk J and van der Mullen J J A M 2012 *J. Phys. D: Appl. Phys.* **45** 335204
- [49] Rahimi S, Jimenez-Diaz M, Hubner S, Kemaneci E H, van der Mullen J J A M and van Dijk J 2014 *J. Phys. D: Appl. Phys.* **47** 125204
- [50] Kabouzi Y, Graves D B, Castanos-Martinez E and Moisan M 2007 *Phys. Rev. E* **75** 016402
- [51] Chen G, Georgieva V, Godfroid Th, Snyders R and Delplancke-Ogletree M-P 2016 *Appl. Cat. B: Environm.* **190** 115
- [52] Richard F, Cormier J M, Pellerin S and Chapelle J. 1996 *J. Appl. Phys.* **79** 2245
- [53] Fridman A, Nester S, Kennedy L A, Saveliev A and Mutaf-Yardemci O et al, 1999 *Prog. Energy Combust. Sci.* **25** 211
- [54] Pellerin S, Richard F, Chapelle J, Cormier J M and Musiol K. 2000, *J. Phys. D: Appl. Phys.*, **33** 2407
- [55] Mutaf-Yardimci O, Saveliev A V, Fridman A A and Kennedy L A 2000 *J. Appl. Phys.* **87** 1632

- [56] Kuznetsova I V, Kalashnikov N Y, Gutsol A F, Fridman A A and Kennedy L A 2002 *J. Appl. Phys.* **92** 4231
- [57] Pellerin S, Cormier J-M, Richard F, Musiol K and Chapelle J 1999 *J. Phys. D: Appl. Phys.* **32** 891
- [58] Gutsol A F and Gangoli S P 2017 *IEEE Trans. Plasma Sci.* (DOI: 10.1109/TPS.2017.2653841)
- [59] Kolev St and Bogaerts A 2015 *Plasma Sources Sci. Technol.* **24** 015025
- [60] Kolev St and Bogaerts A 2015 *Plasma Sources Sci. Technol.* **24** 065023
- [61] Kolev St, Sun SR, Trenchev G, Wang W, Wang HX and Bogaerts A 2017 *Plasma Proc. Polymers* (in press: DOI: 10.1002/ppap.201600110)
- [62] Sun S R, Kolev St, Wang H X and Bogaerts A 2017 *Plasma Sources Sci. Technol.* **26** 015003
- [63] Trenchev G, Kolev St and Bogaerts A 2016 *Plasma Sources Sci. Technol.* **25** 035014
- [64] Sun S R, Wang H X, Mei D H, Tu X and Bogaerts A 2017 *J. CO₂ Utilization* **17** 220
- [65] Wang W, Berthelot A, Kolev St, Tu X and Bogaerts A 2016 *Plasma Sources Sci. Technol.* **25** 065012
- [66] Indarto A, Choi J-W, Lee H and Song H K 2005 *J. Natural Gas Chem.* **14** 13
- [67] Indarto A, Coowanitwong N, Choi J-W, Lee H and Song H K 2008 *Fuel Process. Technol.* **89** 214
- [68] Cenian A, Chernukho A, Borodin V and Sliwinski G 1994 *Contrib. Plasma Phys.* **34** 25
- [69] Cenian A, Chernukho A and Borodin V 1995 *Contrib. Plasma Phys.* **35** 273
- [70] Hokazono H and Fujimoto H 1987 *J. Appl. Phys.* **62** 1585
- [71] Gordiets B F, Osipov A I, Stupochenko E V and Shelepin L A 1973 *Soviet Physics Uspekhi* **15** 759
- [72] Kustova E and Nagnibeda E 2006 *Chem. Phys.* **321** 293
- [73] Rusanov V D, Fridman A A and Sholin G V 1981 *Soviet Physics Uspekhi* **24** 447
- [74] Aerts R, Martens T and Bogaerts A 2012 *J. Phys. Chem. C* **116** 23257
- [75] Kozák T and Bogaerts A 2014 *Plasma Sources Sci. Technol.* **23** 045004
- [76] Kozák T and Bogaerts A 2015 *Plasma Sources Sci. Technol.* **24** 015024
- [77] Ponduri S, Becker M M, Welzel S, van de Sanden M C M, Loffhagen D and Engeln R 2016 *J. Appl. Phys.* **119** 093301
- [78] Pietanza L D, G. Colonna, G. D'Ammando, A. Laricchiuta and M. Capitelli, *Plasma Sources Sci. Technol.* **2015**, *24*, 042002
- [79] Pietanza L D, Colonna G, D'Ammando G, Laricchiuta A and Capitelli 2016 *Chem Phys.* **468** 44
- [80] Pietanza L D, Colonna G, D'Ammando G, Laricchiuta A and Capitelli M 2016 *Phys. Plasmas* **23** 013515
- [81] Pietanza L D, Colonna G, Laporta V, Celiberto R, D'Ammando G, Laricchiuta A and Capitelli M 2016 *J. Phys. Chem A* **120** 2614
- [82] Pietanza L D, Colonna G, D'Ammando G and Capitelli M 2016 *Plasma Phys. Contr. Fusion* **59** 014035
- [83] Capitelli M, Colonna G, D'Ammando G, Hassouni K, Laricchiuta A and Pietanza L D 2017 *Plasma Process Polym.* **14** (in press; DOI: 10.1002/ppap.201600109)
- [84] Koelman P, Heijkers S, Tadayon Mousavi S, Graef W, Mihailova D, Kozák T, Bogaerts A and van Dijk J 2017 *Plasma Process. Polymers* (in press). DOI: 10.1002/ppap.201600155
- [85] Berthelot A and Bogaerts A 2016 *Plasma Sources Sci. Technol.* **25** 045022
- [86] Chen J-L, Wang H-X and Sun S-R 2016 *Chin. Phys. Lett.* **10** 108201
- [87] de la Fuente J F, Moreno S H, Stankiewicz A I and Stefanidis G D 2016 *Reaction Chem Eng* (in press)
- [88] Berthelot A and Bogaerts A *J. Phys Chem C* (submitted)
- [89] Moss M, Yanallah K, Allen R and Pontiga F 2017 *Plasma Sources Sci. Technol.* (in press)
- [90] Yang Y 2003 *Plasma Chem. Plasma Process.* **23** 327
- [91] De Bie C, Verheyde B, Martens T, van Dijk J, Paulussen S and Bogaerts 2011 *Plasma Process. Polym.* **8** 1033
- [92] Luche J, Aubry O, Khacef A and Cormier J M 2009 *Chem. Eng. J.* **149** 35
- [93] Zhou L M, Xue B, Kogelschatz U and Eliasson B 1998 *Energ. Fuel.* **12** 1191
- [94] Machrafi H, Cavadias S and Amouroux J 2011 *J. Phys.: Conf. Ser.* **275** 012016
- [95] Goujard V, Tatibouet J M and Batiot-Dupeyrat C 2011 *Plasma Chem. Plasma Process.* **31** 315

- [96] Wang J G, Liu C J and Eliasson B 2004 *Energ. Fuel.* **18** 148
- [97] Istadi I and Amin N A S 2007 *Chem. Eng. Sci.* **62** 6568
- [98] Kraus M, Egli W, Haffner K, Eliasson B, Kogelschatz U and Wokaun A 2002 *Phys. Chem. Chem. Phys.* **4** 668
- [99] Liu C J, Li Y, Zhang Y P, Wang Y, Zou J, Eliasson B and Xue B 2001 *Chem. Lett.* **12** 1304
- [100] De Bie C, Martens T, van Dijk J, Paulussen S, Verheyde B and Bogaerts A 2011 *Plasma Sources Sci. Technol.* **20** 024008
- [101] Snoeckx R, Aerts R, Tu X and Bogaerts A 2013 *J. Phys. Chem. C* **117** 4957
- [102] Snoeckx R, Zeng Y X, Tu X and Bogaerts A 2015 *RSC Advances* **5** 29799
- [103] Janeco A, Pinhão N R and Guerra V 2015 *J. Phys. Chem. C* **119** 109
- [104] De Bie C, van Dijk J and Bogaerts A 2015 *J. Phys. Chem. C* **119** 22331
- [105] Zhou L M, Xue B, Kogelschatz U and Eliasson B 1998 *Plasma Chem. Plasma Process.* **18** 375
- [106] Nair S A, Nozaki T and Okazaki K 2007 *Chem. Eng. J.* **132** 85
- [107] Goujard V, Nozaki T, Yuzawa S, Ağiral A and Okazaki K 2011 *J. Phys. D: Appl. Phys.* **44** 274011
- [108] Ağiral A, Nozaki T, Nakase M, Yuzawa S, Okazaki K and Gardeniers J G E 2011 *Chem. Eng. J.* **167** 560
- [109] Zhou J, Xu Y, Zhou X, Gong J, Yin Y, Zheng H and Guo H 2011 *ChemSusChem* **4** 1095
- [110] Matin N S and Whitehead J C 2007 *28th ICPIG, July 15-20, 2007, Prague, Czech Republic*, 983.
- [111] Snoeckx R, Ozkan O, Reniers F and Bogaerts A 2017 *ChemSusChem* **10** 409
- [112] De Bie C, van Dijk J and Bogaerts A 2016 *J. Phys. Chem. C* **120** 25210
- [113] Heijkers S, Snoeckx R, Kozák T, Silva T, Godfroid T, Britun N, Snyders R and Bogaerts A 2015 *J. Phys. Chem. C*, **119** 12815
- [114] Snoeckx R, Heijkers S, Van Wesenbeeck K, Lenaerts S and Bogaerts A 2016 *Energy & Environm. Sci.* **9** 999
- [115] Legrand J, Diamy A, Hrach R and Hrachova V 1997 *Vacuum* **48** 671
- [116] Majumdar A, Behnke J F, Hippler R, Matyash K and Schneider R 2005 *J. Phys. Chem. A* **109** 9371
- [117] Pintassiglio C D, Jaoul C, Loureiro J, Belmonte T and Czerwiec T 2007 *J. Phys. D: Appl. Phys.* **40** 3620.
- [118] Jauberteau J L, Jauberteau I, Cinelli M J and Aubreton J 2002 *New J. Phys.* **4** 1.
- [119] Savinov S Y, Lee H, Keun H and Na B 2003 *Plasma Chem. Plasma Process.* **23** 159
- [120] Snoeckx R, Setareh M, Aerts R, Simon P, Maghari A and Bogaerts A 2013 *Int. J. Hydrogen Energy* **38** 16098
- [121] Fridman A 2008 *Plasma Chemistry*, Cambridge University Press, Cambridge
- [122] Bogaerts A, Wang W, Berthelot A and Guerra V 2016 *Plasma Sources Sci. Technol.* **25** 055016
- [123] Britun N, Godfroid T and Snyders R. 2012 *Plasma Sources Sci. Technol.* **21** 035007
- [124] Tu X, Gallon H J and Whitehead J C 2011 Electrical and optical diagnostics of atmospheric pressure argon gliding arc plasma jet *30th Int. Conf. on Phenomena in Ionized Gases (Belfast, UK, 28 August–2 September 2011)*
- [125] Bogaerts A, De Bie C, Snoeckx R and Kozák T, *Plasma Proc. Polymers* (in press: DOI 10.1002/ppap.201600070).
- [126] Grofulovic M, Alves L L and Guerra V 2016 *J. Phys. D: Appl. Phys* **49** 395207
- [127] Phelps Database, www.lxcat.net, retrieved on December 1, 2015
- [128] Lowke J J, Phelps A V and Irwin B W 1973 *J. Appl. Phys.* **44** 4664
- [129] Hake R D Jr., Phelps A V 1967 *Phys. Rev.* **158** 70
- [130] Cosby P C, Helm H 1993 "Dissociation rates of diatomic molecules", Report, AD-A266 464, WL-TR-93-2004
- [131] Itikawa Y 2002 *J. Phys. Chem.* **R31** 749
- [132] Brehmer F, Welzel S, van de Sanden M C M and Engeln R 2014 *J. Appl. Phys.* **116** 123303
- [133] Polak L S, Slovetsky D I 1976 *Int. J. Radiat. Phys. Chem.* **8** 257

- [134] Mahammadunnisa S, Reddy E L, Ray D, Subrahmanyam C and Whitehead J C 2013 *Int. J. Greenh. Gas Control* **16** 361
- [135] Aresta M, Dibenedetto A and Angelini A 2014 *Chem. Rev.* **114** 1709
- [136] Patil B S, Wang Q, Hessel V and Lang J 2015 *Catal. Today* **256** 49
- [137] Scarduelli G, Guella G, Ascenzi D and Tosi P 2011 *Plasma Process. Polym.* **8** 25
- [138] Kim H H, Ogata A and Song Y-H 2011 *IEEE Trans. Plasma Sci.* **39** 2220
- [139] Kim H H and Ogata A 2012 *Int. J. Environ. Sci. Technol.* **6** 43
- [140] Tu X, Gallon H J and Whitehead J C 2011 *IEEE Trans. Plasma Sci.* **39** 2172
- [141] Boisse-Laporte C, Granier A, Dervisevic E, Leprince P and Marec J 1987 *J. Phys. D: Appl. Phys.* **20** 197
- [142] Korolev Y, Frants O, Landl N, Bolotov A and Nekhoroshev V 2014 *Plasma Sources Sci. Technol.* **23** 054016
- [143] Bo Z, Yan J, Li X, Chi Y and Cen K 2008 *Int. J. Hydrog. Energy* **33** 5545
- [144] Rusu I and Cormier J M 2003 *Chem. Eng. J.* **91** 23
- [145] Ouni F, Khacef A and Cormier J M 2006 *Chem. Eng. Technol.* **29** 604
- [146] Aerts R, Snoeckx R and Bogaerts A 2014 *Plasma Process. Polym.* **11** 985
- [147] Pellerin S, Martinie O, Cormier J M, Chapelle J and Lefauchaux P 1999 *High Temp. Mater. Process.* **3** 167
- [148] Zhu J, Sun Z, Li Z, Ehn A, Alden M, Salewski M, Leipold F and Kusano Y 2014 *J. Phys. D: Appl. Phys.* **47** 295203
- [149] Mitsugi F, Furukawa J, Ohshima T, Kawasaki H, Kawasaki T, Aoqui S and Stryczewska H D 2013 *Eur. Phys. J.: Appl. Phys.* **61** 24308
- [150] Smestad G P and Steinfeld A 2012 *Ind. Eng. Chem. Res.* **51** 11828
- [151] Roy S C, Varghese O K, Paulose M and Grimes C A 2010 *ACS Nano* **4** 1259
- [152] Scheffe J R and Steinfeld A 2014 *Mater. Today* **17** 341
- [153] McDaniel A H, Miller E C, Arifin D, Ambrosini A, Coker E N, O'Hayre R, Chueh W C and Tong J 2013 *Energy Environ. Sci.* **6** 2424
- [154] Furler P, Scheffe J R and Steinfeld A 2012 *Energy Environ. Sci.* **5** 6098